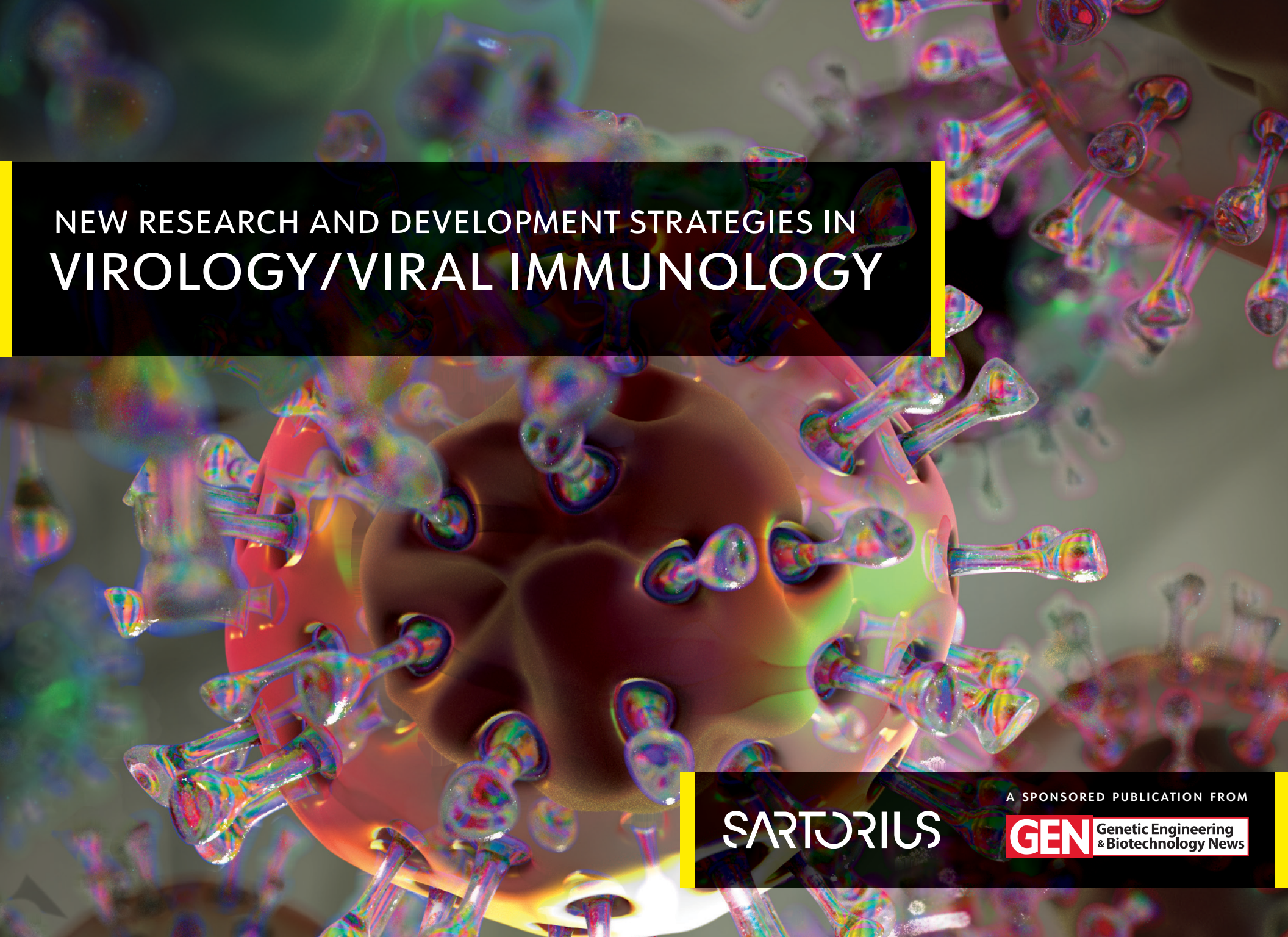

NEW RESEARCH AND DEVELOPMENT STRATEGIES IN VIROLOGY/VIRAL IMMUNOLOGY

A SPONSORED PUBLICATION FROM

SARTORIUS

GEN Genetic Engineering & Biotechnology News

SARTORIUS

Simplifying Progress

Information-Rich Solutions to Transform Biologics Discovery

Sartorius' **Incucyte® Live-Cell Analysis System and Intellicyt® iQue advanced flow cytometry** cell analysis platforms offer unique, high capacity solutions to track complex biological processes and generate deeper, more biologically relevant data for characterizing phenotype, activation and function.

Learn more at: **www.sartorius.com/biologics**

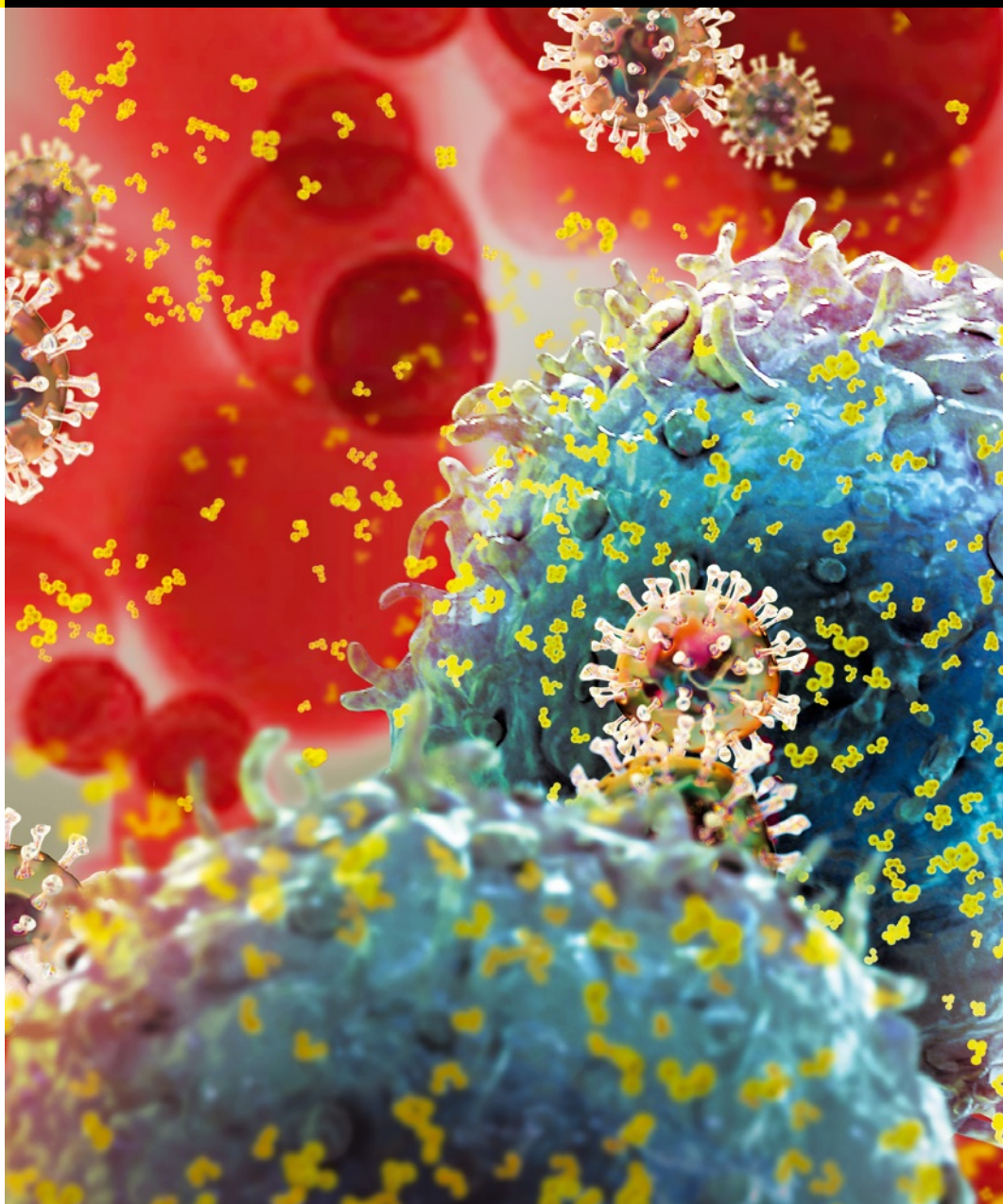

New Research and Development Strategies in Virology/Viral Immunology

SARTORIUS

Vaccines are a potent and cost-effective method of preventing deadly diseases. The recent global outbreak of COVID-19 spurred researchers around the world to quickly create a vaccine to combat the pandemic. However, creation of a human viral vaccine generally takes 10–20 years, but that is the kind of time we do not have when faced with an ongoing pandemic. Even in absence of a pandemic, many researchers consider 10 years too long for a process of creating such vital, life-saving preventive therapies. The goal, then, is to accelerate the viral vaccine development process.

Our current lack of knowledge on the human protective immune response and how it can be induced hampers our ability to create vaccines for many difficult and elusive infectious diseases. To accelerate the process of vaccine creation, we need a deeper understanding of the cellular and molecular mechanisms that drive immune responses against emerging infectious diseases (EIDs). Therefore, researchers need capabilities for high-throughput testing of new vaccine antigens and delivery platforms early in the vaccine creation process. Leading the way are new technologies for developing innovative delivery and formulation.

Sartorius' advanced cell analysis platforms accelerate the discovery and development of new vaccines against viral infections by giving deeper, more relevant data on phenotype, activation, and function so you gain more insight, faster. The iQue® advanced flow cytometry platform enables rapid, high-throughput screening and large scale sample multiplexing across a variety of applications, such as monitoring host – pathogen interactions, antibody library screening, immune response assessment, epitope mapping, and antibody neutralization studies. The Incucyte® Live-Cell Analysis System provides a flexible assay platform that accommodates multiple applications simultaneously, revealing host – virus interactions as well as molecular interactions and mechanisms of infection through virus-modulated cell death, and it enables fast, efficient, and accurate measurement of infectious viral titers, all with multiplate throughput. Analysis is performed with networked, remote access as your cells remain in the physiologically relevant environment of the incubator. Through these groundbreaking innovations that enable the multiplexing of assays and streamlining of workflows for faster time to results, validation by complementary technologies, and robust multiparametric software analysis, Sartorius provides solutions that simplify complexity and expedite discovery for scientists working on the frontline of viral vaccine research.

NEW RESEARCH AND DEVELOPMENT STRATEGIES IN

VIROLOGY/VIRAL IMMUNOLOGY

CONTENTS

Influenza Vaccination Protects Against Pandemic H1N1 Infection in Sickle Cell Disease Mice

By Sean Roberts,[1] Dennis W. Metzger,[1] and Steven M. Szczepanek[2]

1. Department of Immunology and Microbial Disease, Albany Medical College, Albany, New York; 2. Center of Excellence for Vaccine Research, Department of Pathobiology and Veterinary Science, University of Connecticut, Storrs, Connecticut

ABSTRACT

Influenza infection is associated with enhanced pathology in individuals with sickle cell disease (SCD). Despite being a high priority group for annual influenza vaccination, little is known about long-term responses to influenza vaccination in this patient population. To model flu vaccination, we inoculated SCD and wild type (WT) littermate mice with the seasonal flu vaccine [containing pandemic H1N1 (pH1N1) antigen], bled the mice before and after vaccination, and intranasally challenged them with a high dose (400 PFU) of pH1N1 12 weeks later. Both WT and SCD mice were fully protected from infection, and anti-influenza immunoglobulin G titers were significantly elevated in both groups after vaccination. It appears that flu vaccination is effective in SCD mice and our data support the clinical practice of regular flu vaccination in SCD patients.

D-Keine /Getty Images

INTRODUCTION

Infection-associated morbidity and mortality are extremely prevalent in people with sickle cell disease (SCD). This genetic

disorder of the erythrocyte has a profound effect on the immune system, characterized by alterations in splenic architecture, changes in cytokine and immunoglobulin concentrations, and alterations in the distribution of immune cells (11). For the past few decades, enhanced patient care has greatly reduced infection-related burden in the SCD popu- lation; however, infection still remains a major contributor to illness in this group. Influenza virus is one of the most common pathogens found in infected individuals with SCD. The relative incidence is approximately the same for children with SCD as the general population, but the severity of disease is often much worse and is more frequently fatal (5,10). Indeed, hospitalizations for influenza infection have been found to be 56 times higher in children with SCD than those without this genetic disease (1). This is not surprising given that influenza infection has been shown to cause acute chest syndrome, acute marrow suppression of red blood cell pro- duction, pain crisis, and hematuria in children with SCD (6), which are all sequelae not endured by infected individuals who do not have SCD. Furthermore, a recent study has demonstrated that transgenic SCD mice recapitulate severe influenza infection when they are inoculated with the pandemic H1N1 (pH1N1) strain of the virus (7). Given the severity of influenza infection in those with SCD, we sought to determine the relative efficacy of influenza vaccination in SCD mice.

INFLUENZA VACCINATION RESPONSES IN SCD MICE

Most current clinical guidelines recommend that vaccination against influenza virus should occur on an annual basis in people with SCD. In light of previous observations that vaccination responses are aberrant in SCD mice (12), we developed a mouse model of influenza vaccination and challenge using the seasonal influenza vaccine (Fluzone; Sanofi Pasteur, Inc.) and mouse-adapted strain of pH1N1 influenza virus (9). A 8- to 12-week-old female SCD and littermate wild type (WT) mice (8) were intramuscularly vaccinated with 4.5 mg of vaccine [containing 1.5 mg of CA07 2009 HA (4)] on weeks 0 and 3 (nonvaccinated WT naive mice were included as controls), i.n. challenged 12 weeks after the initial priming dose with 400 PFU of pH1N1 (four times higher than the LD100 for this strain in WT mice, data not shown), and mortality (Fig. 1A) and weight loss (Fig. 1B) were assessed. Mice were bled on weeks 0 and 4 and anti-pH1N1 titers were determined by enzyme- linked immunosorbent assay (Fig. 1C). Mice were housed under specific pathogen-free conditions and all work was conducted under an approved Institutional Animal Care and Use Committee protocol from Albany Medical College. Vaccinated WT and SCD mice survived infection

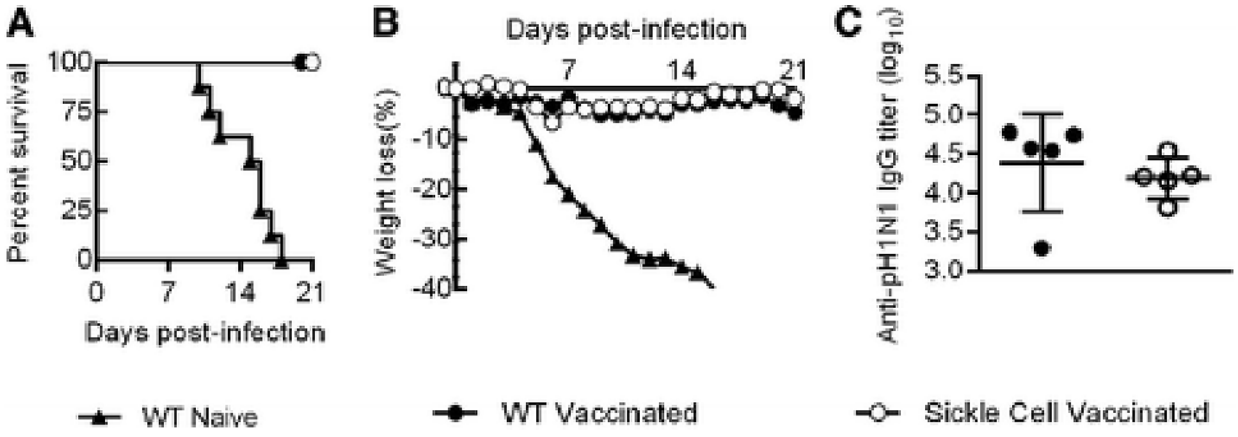

FIG. 1. Influenza vaccination and challenge model. (A) Mortality curve depicting percentage survival after intranasal challenge with mouse-adapted pH1N1 in vaccinated mice. (B) Curves showing percentage weight lost after challenge with pH1N1. (C) Anti-pH1N1 IgG titers were measured by ELISA. Points represent the mean value. ELISA statistics were assessed by the Mann-Whitney U test. ELISA, enzyme-linked immunosorbent assay; IgG, immunoglobulin G; pH1N1, pandemic H1N1; WT, wild type.

and had similar endpoint anti-pH1N1 immunoglobulin G (IgG) titers 4 weeks after vaccination (as determined using a Mann-Whitney U test), whereas naive WT mice all succumbed to infection by day 18 postinfection and had no detectable anti-pH1N1 IgG titers. We again bled surviving mice 23 weeks after priming (11 weeks after infection) and determined that anti-influenza IgG titers were maintained in WT mice and increased twofold in SCD mice (data not shown), indicating that long-term protective humoral responses to influenza virus are possible in SCD mice, despite their immunological abnormalities. Both vaccinated groups did lose weight after infection, indicating that the infection was successful in these mice.

CONCLUSION

Our results show that flu vaccination is effective at protecting SCD mice from influenza infection. This is somewhat surprising as these data are in stark contrast to reports from us (3,13) and others (2), showing that pneumococcal vaccine responses are not sustained in SCD mice. Our data, taken together with those from Karlsson *et al.* (7), support the clinical practice of routinely administering the flu vaccine in SCD patients to protect against severe disease associated with influenza infection. ■

ACKNOWLEDGMENTS

The authors thank Sharon Salmon for technical assistance with the experiments and members of the Thrall laboratory at UCHC for insightful conversations regarding this line of research.

AUTHOR DISCLOSURE STATEMENT

The authors declare no financial or nonfinancial competing interests.

REFERENCES

1 Bundy DG, Strouse JJ, Casella JF, *et al.* Burden of influenza-related hospitalizations among children with sickle cell disease. Pediatrics 2010;125:234-243.

2 Carter R, Wolf J, van Opijnen T, *et al.* Genomic analyses of pneumococci from children with sickle cell disease expose host-specific bacterial adaptations and deficits in current interventions. Cell Host Microbe 2014;15:587-599.

3 Cotte C, and Szczepanek SM. Peritoneal B-1b and B-2 B-cells confer long-term protection from pneumococcal serotype 3 infection after vaccination with Prevnar-13 and are defective in sickle cell disease mice. Vaccine 2017;35:3520-3522.

4 Furuya Y, Kirimanjeswara GS, Roberts S, *et al.* Defective anti-polysaccharide IgG vaccine responses in IgA deficient mice. Vaccine 2017;35:4997-5005.

5 George A, Benton J, Pratt J, *et al.* The impact of the 2009 H1N1 influenza pandemic on pediatric patients with sickle cell disease. Pediatr Blood Cancer 2011;57:648-653.

6 Jacobs JE, Quirolo K, and Vichinsky E. Novel influenza A (H1N1) viral infection in pediatric patients with sickle-cell disease. Pediatr Blood Cancer 2011;56:95-98.

7 Karlsson EA, Oguin TH, Meliopoulos V, *et al.* Vascular permeability drives susceptibility to influenza infection in a murine model of sickle cell disease. Sci Rep 2017;7:43308.

8 Ryan TM, Ciavatta DJ, and Townes TM. Knockout-transgenic mouse model of sickle cell disease. Science 1997;278:873 876.

9 Sun K, Ye J, Perez DR, *et al.* Seasonal FluMist vaccination induces cross-reactive T cell immunity against H1N1 (2009) influenza and secondary bacterial infections. J Immunol 2011; 186:987-993.

10 Strouse JJ, Reller ME, Bundy DG, *et al.* Severe pandemic H1N1 and seasonal influenza in children and young adults with sickle cell disease. Blood 2010;116:3431-3434.

11 Szczepanek SM, McNamara JT, Secor ER Jr, *et al.* Splenic morphological changes are accompanied by altered baseline immunity in a mouse model of sickle-cell disease. Am J Pathol 2012;181:1725-1734.

12 Szczepanek SM, Secor ER Jr, Bracken SJ, *et al.* Transgenic sickle cell disease mice have high mortality and dysregulated immune responses after vaccination. Pediatr Res 2013;74: 141-147.

13 Szczepanek SM, Roberts S, Rogers K, *et al.* Poor long-term efficacy of Prevnar-13 in sickle cell disease mice is asso- ciated with an inability to sustain pneumococcal-specific antibody titers. PLoS One 2016;11:e0149261.

Microparticle Release from Cell Lines and Its Anti-Influenza Activity

Saharat Jantaratrirat[1], Chompunuch Boonarkart[1], Kanyarat Ruangrung[1], Prasert Auewarakul[1], and Ornpreya Suptawiwa[2]

1. Department of Microbiology, Faculty of Medicine Siriraj Hospital, Mahidol University, Bangkok, Thailand; 2. Faculty of Medicine and Public Health, HRH Princess Chulabhorn College of Medical Science, Chulabhorn Royal Academy, Bangkok, Thailand.

ABSTRACT

Microparticles (MPs) are vesicles that are released by budding from plasma membrane of living cells. Recently, the role of MPs in antiviral activity has been proposed. We investigated quantity and anti-influenza activity of MPs from human alveolar epithelial cells A549, human bronchial epithelial cells BEAS-2B, human colon adenocarcinoma cells HT-29, and the human lung fibroblast cells MRC-5. MPs were found from all four cell lines. However, anti-influenza activity against an H1N1 influenza virus was found only from MPs of A549 and BEAS-2B. BEAS-2B cell differentiation did not increase MP release. Methyl-β-cyclodextrin (MβCD)

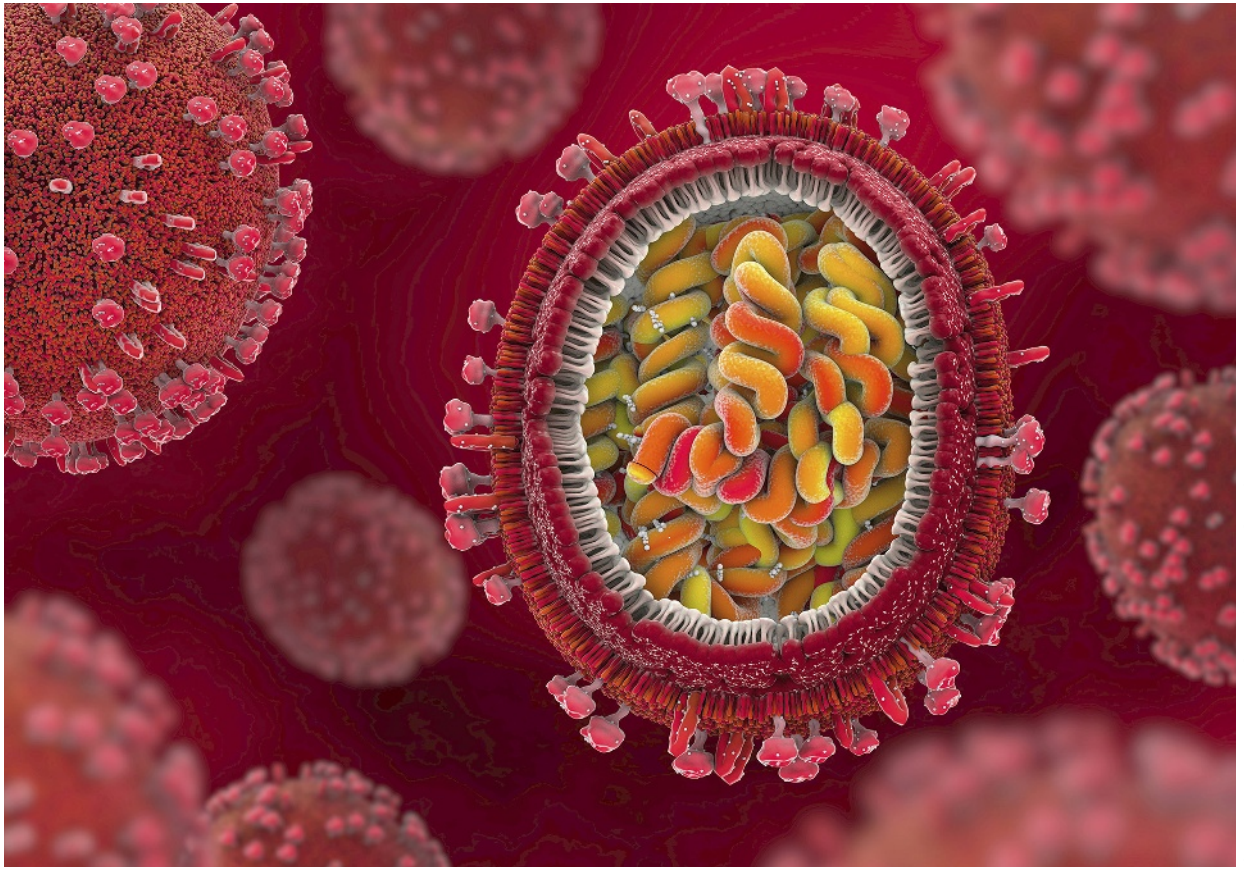

Getty Images / Christoph Burgstedt / Science Photo Library

increased MP release and anti-influenza activity in HT-29 and A549. MP release increased after calcium ionophore A23187 treatment in three cell lines but only in HT-29 after forskolin treatment. These findings provide *in vitro* data supporting the role of MPs as an innate defense against influenza virus and as an approach to enhance the defense.

INTRODUCTION

Cells secrete many different kinds of vesicles, termed extracellular vesicles (EV). The term EV covers a broad range of secreted vesicles, including exosomes, microparticles (MPs), and apoptotic bodies. MPs refer to phospholipid vesicles from 100 to 1,000 nm in diameter that are released by budding from plasma membrane of living cells and express antigens specific to their parental cells (19). Many cell types have been reported to release MPs. For example, endothelial cells (2), vascular smooth muscle cells (4), platelets (31), monocytes (22), and erythrocytes (10). MPs also have been isolated from bronchoalveolar lavage (BAL) fluid (7) and urine (24).

MPs have been shown to play a role in intercellular exchange of biological signals and information (19). Another role of MPs in antiviral activity has been proposed. It has been reported that the vesicles secreted by human tracheobronchial epithelial cells have a neutralizing effect on human influenza A virus (IAV) (14), and our recent data have shown anti-influenza activity of MPs isolated from human BAL (29). In the initial step of infection, IAV hemagglutinin (HA) protein binds to sialic acid residues on the respiratory epithelial cell, triggering endocytosis of the virion into the host cell. Since MPs express surface molecules specific to their parental cells, it is possible that MPs from the respiratory epithelial cells contain IAV receptors that can act as a decoy receptor to prevent the binding of viral HA on cell surface. However, data of MPs released from cell lines are limited.

Generation and release of MPs occur during different biological processes, including stimulation with high shear stress as present in arteries with a severe stenosis, cellular differentiation, senescence, apoptotic cell breakdown, or exposed to proinflammatory, prothrombotic, or proapoptotic substances (19). It is generally assumed that MPs form when the asymmetrical distribution of lipids between the inner and outer leaflets of a plasma membrane is lost (6).

In resting cells, phosphatidylserine (PS) is located almost exclusively in the inner leaflet of the plasma membrane (30). The transbilayer lipid redistribution is under the control of three translocase proteins: flippase, an inward-directed PS-specific pump; floppase, an outward-directed PS-specific pump; and a lipid scramblase, promoting unspecific bidirectional redistribution across the bilayer (34). A significant increase of cytosolic Ca^{2+} accompanying cell stimulation may

lead to the collapse of the membrane asymmetry by activation of calcium-dependent enzymes such as scramblase and floppase (21). Increase in cytosolic Ca^{2+} also promotes disassembly of the cytoskeleton through protein-degrading enzymes, for example, calcium-activated calpains (13).

In vitro release of MPs can be induced by various compounds, for instance, calcium ionophore A23187, a mobile ion carrier that is used for increasing intracellular Ca^{2+} levels (8); and forskolin, a herbal extract commonly used as a specific activator of the cyclic AMP (cAMP) (11,33). High intracellular levels of cAMP can lead to increased intracellular Ca^{2+} levels (16,17). Moreover, cyclodextrins (CDs), nonreducing cyclic glucose oligosaccharides, are used to selectively extract membrane cholesterol, the major lipid constituent of the plasma membrane of mammalian cells (20). The disturbances of lipid rafts by removing cholesterol from cell membranes by methyl-β-cyclodextrin (MβCD), a derivative of CDs, have been suggested to induce MP release (25). However, data of MP induction by calcium ionophore, MβCD, A23187, and forskolin in other cells are still limited.

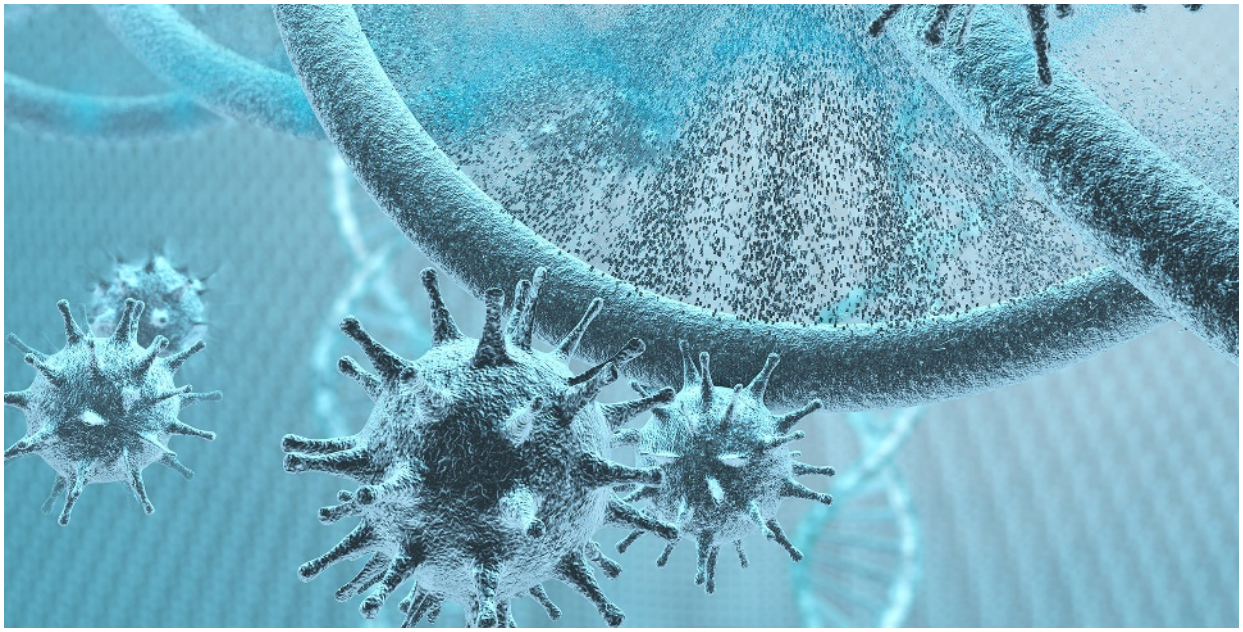

Fatido /Getty Images

In this study, we hypothesized that MPs may relate to mucosal defense against viral infection, since the mucosa is a membrane that consists of layers of epithelial cells. Thus, we selected three epithelial cell lines, including human lung alveolar epithelial cell line A549, transformed bronchial epithelial cell line BEAS-2B, human colon adenocarcinoma cells line HT-29, and nonepithelial cells, the human lung fibroblast cell line MRC-5 to determine the differences in MP release and anti-influenza activity. We also challenged the cells with various concentrations of MβCD, calcium ionophore A23187, and forskolin to assess their ability to induce MP release.

MATERIALS AND METHODS

Cell lines

Human lung alveolar epithelial cell line A549 (lung adenocarcinoma, ATCC CCL-185) was cultured in Dulbecco's modified Eagle's medium (DMEM; Sigma) supplemented with heat-inactivated 10% fetal bovine serum (FBS; Gibco); transformed bronchial epithelial cell line BEAS-2B (human bronchial epithelium, ATCC CRL-9609) was cultured in bronchial epithelial growth medium (BEGM; Lonza); human colon adenocarcinoma cell line HT-29 (colon adenocarcinoma, ATCC HTB-38) was cultured in McCoy's 5A media (Gibco) supplemented with 10% heat-inactivated FBS; and the human lung fibroblast cell line MRC-5 was cultured in minimum essential medium (MEM; Gibco) supplemented with 2 mM sodium pyruvate, 0.1 mM nonessential amino acids, and heat-inactivated 10% FBS.

Viral strains

The influenza viruses used in this study were the 2009 pandemic H1N1 (pdmH1N1) influenza virus A/Thailand/MVCU-013/2009 propagated in Madin–Darby canine kidney (MDCK) cells and a reverse genetic virus containing the monobasic cleavage site, HA gene from a highly pathogenic avian influenza A/Thailand/1(KAN-1)/2004 (H5N1) virus, and seven genes from A/Puerto Rico/8/34 (H1N1) virus (rVac-H5) (28).

Air–Liquid interface culture

Cells were cultured on 12 mm polyester Transwell inserts with a pore size of 0.4 μm (Corning). BEAS-2B cells were plated at 100,000 cells per insert in growth factor-supplemented medium (BEGM) (Lonza Walkersville, Inc.). When confluent (~3 days), medium from apical and basal chambers was removed and differentiation medium (BEDM) was added to the basal chamber only. Medium was replaced every 48 h. Differentiated cell was tested after an incubation period of 21 days (27).

Lectin staining

Cells were trypsinized and cell suspensions were then blocked for nonspecific binding with 3% bovine serum albumin (Sigma) in 1× phosphate-buffered saline (PBS) for 30 min. After discarding blocking solution, the cell suspensions were incubated with 10 μg of FITC-conjugated *Maackia amurensis* lectin MAA I or *Sambucus nigra* lectin SNA (Vector Laboratories) in blocking solution for 30 min at room temperature, then washed three times with PBS, and finally, stained cells were fixed with 1% paraformaldehyde (PFA) in 1× PBS. Flow cytometry measurements were performed immediately using an FACSCalibur instrument and CellQuest software (Becton Dickinson).

MP collection

Cells were maintained at 37°C in 5% CO_2 before being seeded onto 12-well plates at a density of 5×10^5 cells per well. After overnight incubation, culture supernatant was removed and 1 mL of fresh media

with or without various concentrations of testing compound, including MβCD (Acros Organics), calcium ionophore A23187 (Sigma), and forskolin (Sigma), were added before incubating at 37°C in 5% CO_2. Culture supernatant was collected and cell debris was removed by centrifugation two times at 200 *g* for 5 min. MPs were isolated from culture supernatant by centrifugation at 20,000 *g* for 120 min at 4°C.

Apoptotic body staining

For apoptotic bodies using as positive control, HT-29 cells were treated with hydrogen peroxide in serum-free medium for 24 h. The cell culture supernatants were collected and centrifuged two times at 200 *g* for 10 min to remove cells and cell debris. MP samples and supernatant from the HT-29 cells were stained with 3 μL of annexin V-FITC in annexin V buffer in the dark at room temperature for 15 min and subsequently stained with 1 μg/mL of propidium iodide (PI) in the dark at room temperature for 15 min. The stained samples were analyzed immediately using an FACSCalibur instrument and CellQuest software (Becton Dickinson).

Flow cytometry and MP analysis

According to the property of MPs that express PS on their surface, we stained MPs with annexin V, a specific marker for PS. Isolated MPs resuspended in 100 μL of culture medium were stained with 3 μL annexin V-FITC (BD Pharmingen) in a tube that has 20,000 particles of 1.34 μM latex beads (SPHERO™ Fluorescent Particles), diluted with twofold annexin V-FITC binding buffer (BD Pharmingen), and incubated for 15 min in the dark at room temperature. Flow cytometry measurements were performed immediately using an FACSCalibur instrument and CellQuest software (Becton Dickinson). MPs were defined as those smaller than the latex bead and positively stained for annexin V. Absolute MP count per microliter was calculated by using the formula (number of MPs counted/number of beads counted)χ (total number of beads in tube/volume of tested MPs).

Hemagglutination inhibition assay

MP samples were twofold serially diluted in 1 × PBS. Each diluted MP was mixed with four hemagglutination U/25 μL of influenza virus A/Thailand/MVCU-13/2009 (H1N1) or rVac-H5 virus in a 96-well U-shaped microtiter plate. The virus–MP mixture was incubated at room temperature for 30 min. Then, 50 μL of 0.5% goose red blood cells was added to the virus–MP mixture and was incubated at 4°C for 30 min. HI titers were read as reciprocal of the highest dilution with complete inhibited hemagglutination. Each MP sample was tested in duplicate.

Microneutralization assay

MP samples were twofold serially diluted in MEM plus 1 mM TPCK-treated trypsin,

and then, 50 μL of each MP dilution was mixed with an equal volume of the test virus at a concentration of 25 TCID50/50 μL. The virus–serum mixture was incubated at 37°C for an hour. A one hundred microliter of the mixture was inoculated onto an MDCK cell in a 96-well tissue culture plate. After an overnight incubation at 37°C, the tissue culture plate was washed and fixed with 80% cold acetone in 1× PBS. The assays were run in duplicate. The reaction plate was tested by ELISA to determine the amount of influenza nucleoprotein produced in the infected MDCK cells using an antiviral nucleoprotein monoclonal antibody (Milipore) as the primary antibody, a peroxidase-conjugated antibody (Dako) as secondary antibody, and TMB (KPL, Inc., Gaithersburg, MD) as the chromogenic substrate. The reaction plate was read under a spectrophotometer at the wavelengths of 450 and 630 nm. The neutralizing (NT) titer was defined as the reciprocal of the highest MP dilution that reduces more than 50% of the amount of viral nucleoprotein in the reaction wells compared with the virus control wells.

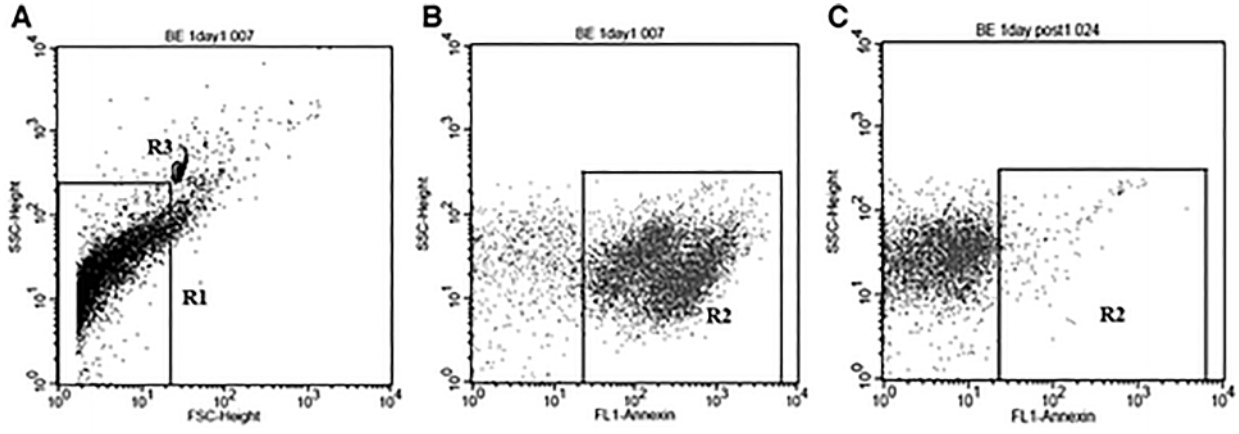

FIG. 1. Flow cytometry analysis of MPs from culture supernatant of cell culture. In region R1 **(A)**, the population that was smaller than 1.34 μM latex beads (R3) by size on FSC/SSC cytogram was gated. Only events included within gate R1 were further identified by their SSC/annexin FITC. In region R2, the population of MPs was determined as the annexin-positive population **(B)** that was absent after degradation of MPs by adding 0.1% Triton X-100 nonionic detergent **(C)**. FSC, forward scatter; MP, microparticle; SSC, side scatter.

Statistical analysis

Data are presented as means and SEMs. Groups were compared using the Student *t* test and one-way ANOVA with Tukey's multiple comparisons test. $p < 0.05$ was considered significant.

RESULTS

MPs from A549, BEAS-2B, HT-29, and MRC-5 cells and their anti-influenza activity

We investigated the difference in MPs released from epithelial cells among alveolar epithelial cells A549, bronchial epithelial cells BEAS-2B, colonic epithelial cells HT-29, and the difference between epithelial cells and lung fibroblast cells MRC-5. MP samples were quantified

and assessed for anti-influenza activity. MP samples were analyzed by flow cytometry as shown in A; on a cytogram of forward scatter versus side scatter (SSC), the population that was smaller than 1.34 μM latex beads (R3) was gated (R1). In Figure 1B, only events included within gate R1 were further identified by their SSC/annexin FITC. The population of MPs was determined as the annexin-positive population that was absent after degradation of MPs by adding 0.1% Triton X-100 nonionic detergent that solubilizes cell membrane but does not disrupt protein aggregates (1) as shown in Figure 1C.

We showed that MPs were found in cell culture supernatant of A549, BEAS-2B, HT-29, and MRC-5 cells as shown in Figure 2. Among these cells, BEAS-2B cells showed the highest MP release followed by HT-29, A549, and MRC-5 cells. MPs from BEAS-2B and A549 cells had a maximum level at 30 min and 3 h, respectively, and persisted up to 24 h. However, MPs from HT-29 and MRC-5 cells continuously increased from 0 to 24 h. MPs from cell culture supernatant of BEAS-2B and A549 cells also had anti-influenza activity against H1N1 virus. However, anti-influenza activity was not found in MPs from HT-29 and MRC-5 cells (Table 1). BEAS-2B cell differentiation induced by culturing at an air–liquid interface did not increase MP release and anti-influenza activity compared with normal BEAS-2B cells as shown in Figure 2 and Table 1, respectively. Anti-influenza activity against H5N1 virus was also found in MPs from BEAS-2B and HT-29 cells (Table 1).

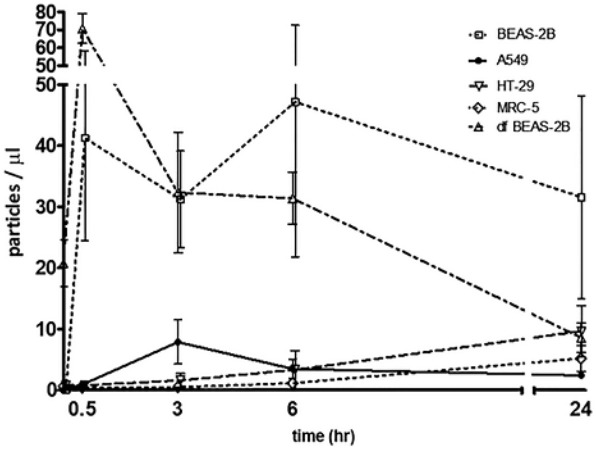

FIG. 2. MPs released from A549, HT-29, MRC-5, BEAS-2B, and differentiated BEAS-2B cells were cultured on 12-well plate for 24 h. Then, culture supernatant was removed and 1 mL of fresh media was added before incubating at 37°C, in 5% CO_2. Culture supernatants were collected at 0, 30 min, 3, 6, and 24 h. MPs were quantified by flow cytometry. The experiments were performed in triplicate. Bars and errors represent mean ± SEM.

The sialic acid expression on the membrane of BEAS-2B, A549, HT-29, and MRC-5 cells

We next sought to investigate the expression levels of sialic acid on BEAS-2B, A549, HT-29, and MRC-5 cells. The cells were stained with FITC-conjugated lectin MAA I or SNA, specific toward α2,3- or α2,6-linked sialic acid, respectively. The results showed that compared with BEAS-2B, A549 cell has lower fluorescence intensity in MAA I and has similar level of fluorescence intensity in SNA, whereas HT-29 and MRC-5 have lower fluorescence intensity than BEAS-2B in both MAA I and SNA (Fig. 3). We further normalized MP

concentration to 10 MP/μL and performed HI assay to confirm that the difference in sialic acid expression correlated with anti-influenza activity. The HI titer result indicated that MPs from BEAS-2B and A549 cells had anti-influenza activity against H1N1 influenza virus. However, only MPs from BEAS-2B had anti-influenza activity against H5N1 influenza virus (Table 2). The discrepancy result of anti-influenza activity against H5N1 between BEAS-2B and HT-29 in Tables 1 and 2 suggested that the inhibition activity from MPs correlated to the levels of (2–3) linked sialic acid expression on MP surface from both cell types.

MP induction by MβCD and calcium ionophore A23187

To enhance innate mucosal immune defense through MP induction, epithelial cells should be the target cells. Thus, we chose only epithelial cells for investigation of the compounds that might increase MP release. The MPs from the cells that were exposed to various concentrations of MβCD and calcium ionophore A23187 for 1 h were quantified and assessed for anti-influenza activity. After being exposed to MβCD for 1 h, MP release was significantly increased in HT-29 and A549 cells but not in BEAS-2B cells (Fig. 4). Concordantly, anti-influenza

Table 1. HI Titer Against H1N1 Influenza Virus Strain A/Thailand/MVCU-13/2009 or Reverse Genetic Virus of H5N1 [(A/Thailand/1(KAN-1)/2004) and rVac-H5 as Described in Detail in *Materials and Methods*; rVac-H5] of MPs Released from A549, HT-29, MRC-5, BEAS-2B, and Differentiated BEAS-2B Cells at 0, 30 min, 3, 6, and 24 H

	HI titer against H1N1 influenza virus					HI titer against rVac-H5 HA virus			
Time	**A549**	**HT-29**	**MRC-5**	**BEAS-2B**	**dfBEAS-2B**	**A549**	**HT-29**	**MRC-5**	**BEAS-2B**
Media	Negative	Negative	Negative	Negative	Negative	Negative	Negative	Negative	Negative
0 min	Negative	Negative	Negative	1	1	Negative	Negative	Negative	Negative
30 min	1	Negative	Negative	1	1	Negative	Negative	Negative	1
3 h	1	Negative	Negative	1	1	Negative	Negative	Negative	1
6 h	1	Negative	Negative	1	1	Negative	Negative	Negative	1
24 h	1	Negative	Negative	1	1	Negative	1	Negative	1

Results are representative of three experiments. MP, microparticle.

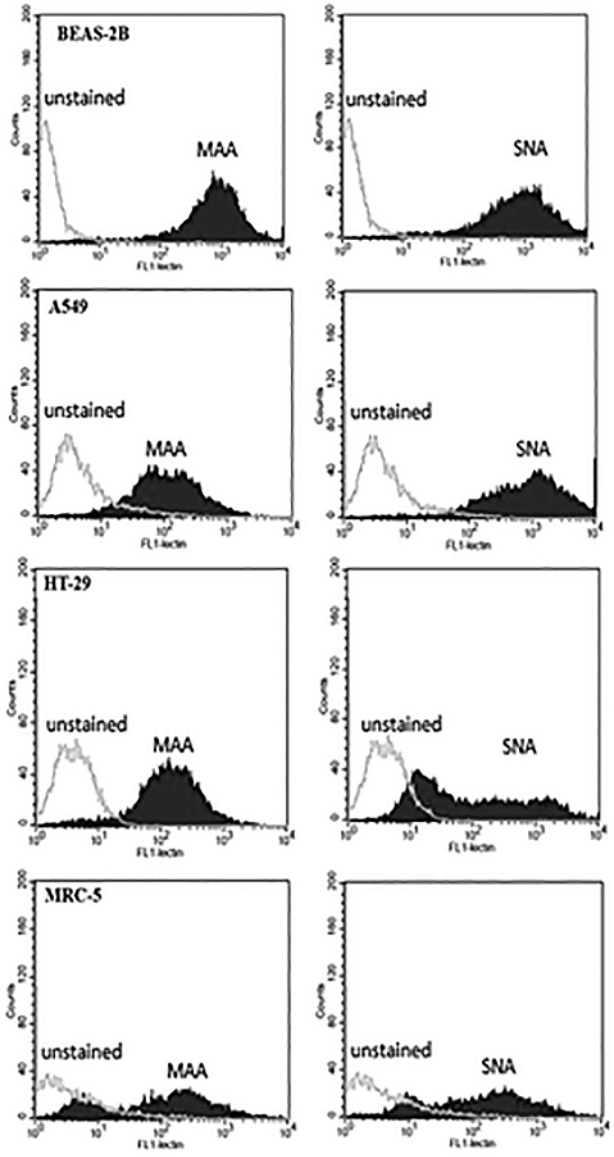

activity by the HI and NT assays of MPs from HT-29 and A549 treated with MβCD were increased compared with that of cell control (Fig. 5). In contrast, after being exposed to calcium ionophore A23187 for 1 h, BEAS-2B showed a marked increase in MP release, whereas only a modest increase was observed in A459 and HT-29 (Fig. 6).

MP induction by forskolin, salbutamol, and aminophylline

Among HT-29, BEAS-2B, and A549 cells, forskolin treatment increased MP release and anti-influenza activity only in HT-29 cells (Fig. 7 and Table 3). Aminophylline and salbutamol are bronchodilator drugs that increase intracellular levels of cAMP through different mechanisms (9,12). We compared the ability of MP induction between forskolin with salbutamol and aminophylline in A549 cells. MP samples from treated cells were quantified and assessed for anti-influenza activity. The results showed that there was no difference in either MPs released (Fig. 8) or HI titer against influenza virus (A/Thailand/MVCU-13/2009) (data not shown).

FIG. 3. Flow cytometry histogram profile of BEAS-2B, A549, HT-29, and MRC-5 cells that were unstained or stained with 1 μg of FITC-conjugated lectin MAA I (*left panel*) or SNA (*right panel*) for 30 min at room temperature.

Verification of MP preparation

To investigate whether MP fraction contains apoptotic bodies, we double stained the MP samples with annexin V and PI. MP population in gate R2 of Figure 1B was further observed for PI intensity on histogram plot compared with the apoptotic body control obtained from the supernatant of H_2O_2-treated cells. The result showed the PI peak of apoptotic bodies in supernatant of H_2O_2-treated cells (Fig. 9A), which was absent in MP population of A549 and HT-29 cells cultured in normal condition (Fig. 9B, C) and treated with MβCD (Fig. 9D, E). These

indicated that the MP samples did not contain a significant amount of apoptotic bodies, and the annexin V staining in MP preparation really represented MPs. To clarify whether there was anti-influenza activity of exosomes from cell lines, the MP pellets and supernatants after centrifugation at 20,000 *g* for 2 h were tested for anti-influenza activity. The HI activity was only present in the MP pellets of cell treated with 25 mM MβCD for 1 h (Table 4).

DISCUSSION

We have recently found anti-influenza activity from MPs isolated from human BAL (29). Thus, in an effort to provide *in vitro* data supporting the role of MPs as an innate defense against influenza virus, we investigated quantity and anti-influenza activity of MPs from culture supernatant of A549, BEAS-2B, HT-29, and MRC-5 cells by performing flow cytometry and HI assay. In this study, MPs were isolated from culture supernatant by centrifugation at 20,000 *g* for 2 h. At this centrifugation speed, MPs will be precipitated while exosomes that require higher speed (19) were still suspended in culture supernatant and no anti-influenza activity was found from culture supernatants after the centrifugation. Moreover, our previous publication did not observe a significant amount of 50 ± 100 nm particles; range of exosome size in human BAL by electron microscopy and the exosome fraction by ultracentrifugation did not show anti-influenza activity (29). It suggests that epithelial cells released exosomes in low level and exosomes were not an important part of the anti-influenza activity. Since annexin V can stain both the MPs and apoptotic bodies, it is possible that the fraction of MPs using FACS contain apoptotic bodies. However, we did not observe apoptotic bodies from the MP sample isolated from cells that were cultured in normal condition and treated with MβCD.

We demonstrated that all four tested cell lines released MPs in normal culture condition in different quantities. BEAS-2B showed the highest MP release and anti-influenza activity, but anti-influenza activity could only be detected in MPs from BEAS-2B and A549 cells. BEAS-2B did not increase MP release after inducing cell differentiation by culturing at an air–liquid interface. Conversely, the level of MPs from differentiated BEAS-2B cells decreased at 3, 6, and 24 h. It may be because the differentiated BEAS-2B cells produce a mucin (32) and secreted MPs may be adsorbed by mucin, contributing to the decrease of MP level.

The levels of sialic acid expression on each cell line partially explained the difference in the levels of anti-influenza activity. BEAS-2B cells strongly expressed both α2,6- and α2,3-linked sialic acids and their MP showed antiviral activity against both H1N1 and H5N1, which is known to bind α2,6- and α2,3-linked sialic acids, respectively. In contrast, A549

cells strongly expressed only α2,6-linked sialic acid and showed antiviral activity only against H1N1 virus, whereas MRC-5 cells expressed little of both sialic acids and showed no antiviral activity against both types of viruses. Although HT-29 cells showed weak staining for both types of sialic acids, the signal of α2,3-linked sialic acid was higher than that of α2,6-linked sialic acid and their MPs showed some activity against H5N1 virus. The comparable levels of antiviral activity against H1N1 virus between MPs from BEAS-2B and A549 cells are surprising since the level of MPs in supernatant of BEAS-2B cells was much higher and both cells expressed similar levels of α2,6-linked sialic acid. Other factors may contribute to the relative antiviral activity between MPs from the two cell lines. Alternatively, it is possible that the quantification of MPs by annexin V staining may not include all MPs as there were reports of annexin V negative MPs (3) and different levels of annexin V-negative MPs

Table 2. HI Titer Against H1N1 Influenza Virus Strain A/Thailand/MVCU-13/2009 or Reverse Genetic Virus of H5N1 [(A/Thailand/1(KAN-1)/2004) as Described in Detail in Materials and Methods; rVac-H5] of MPs from BEAS-2B, A549, HT-29, and MRC-5 Cells That Normalized Concentration to 10 MP/μl

Cell lines	rVac-H5 HA virus	H1N1 influenza virus
BEAS-2B	1	1
A549	Negative	2
HT-29	Negative	Negative
MRC-5	Negative	Negative

Results are representative of three experiments.

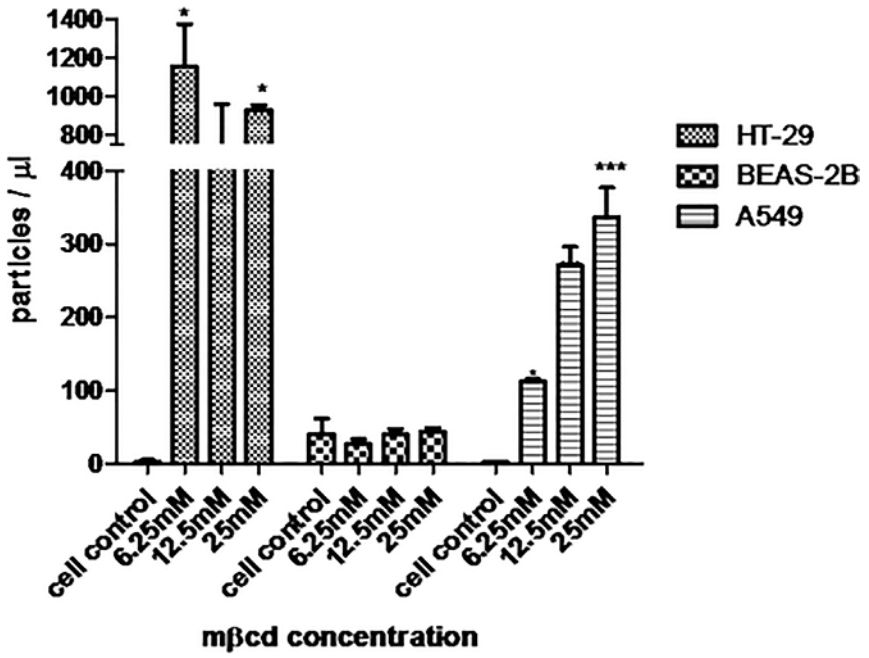

FIG. 4. MP release from HT-29, BEAS-2B, and A549 after MβCD treatment. Cells were cultured on 12-well plate for 24 h. Then, culture supernatant was replaced with 1 mL of media in the presence of MβCD 6.25, 12.5, and 25 mM before incubating at 37°C, in 5% CO_2. Culture supernatant was collected at 60 min after incubation. MPs were quantified by flow cytometry. Bar graphs represent the mean ± SEM for three experiments. Statistical significance was determined by one-way ANOVA with Tukey's test for multiple comparisons (*$p < 0.05$ and ***$p < 0.00$). MβCD, methyl-β-cyclodextrin.

from different cell types (23).

We demonstrated that MβCD, forskolin, and calcium ionophore A23187 can increase MP release and anti-influenza activity especially in HT-29 cells. It may be a specific property of HT-29 cells that allow efficient stimulation of MP release, even though it releases low level of MPs in a normal culture condition.

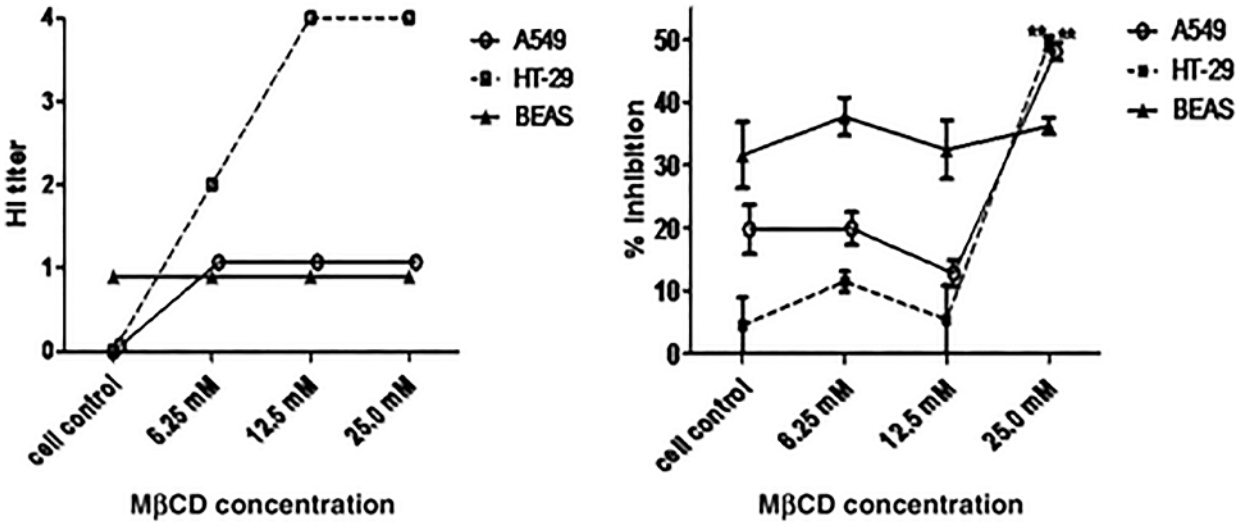

FIG. 5. Neutralization and HI activity against H1N1 influenza virus strain A/Thailand/MVCU-13/2009 of MP release from A549, HT29, and BESA-2B cells after treatment with MβCD 6.25, 12.5, and 25 mM for 1 h. Graphs represent the mean ± SEM of triplicate results. Statistical significance was determined by one-way ANOVA with Tukey's test for multiple comparisons

Table 3. HI Titer Against H1N1 Influenza Virus Strain A/Thailand/MVCU-13/2009 of MP Release from A549, HT-29, and BEAS-2B Cells After Treatment with Forskolin 1, 2, and 5 μM for 1 H

	Forskolin		
Concentration	***HT-29***	***BEAS-2B***	***A549***
Media	Negative	Negative	Negative
Cell control	Negative	Negative	Negative
1 μM	Negative	Negative	Negative
2 μM	Negative	Negative	Negative
5 μM	1	Negative	Negative

Results are representative of three experiments

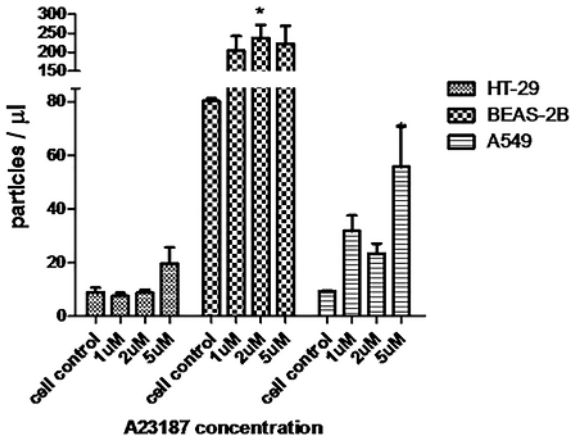

FIG. 6. MP release from HT-29, BEAS-2B, and A549 after calcium ionophore A23187 treatment. Cells were cultured on 12-well plate for 24 h. Then, culture supernfig. 5atant was replaced with 1 mL of media in the presence of calcium ionophore A23187 1, 2, and 5 μM before incubating at 37°C, in 5% CO_2. Culture supernatant was collected at 60 min after incubation. MPs were quantified by flow cytometry. Bar graphs represent the mean ± SEM for three experiments. Statistical significance was determined by one-way ANOVA with Tukey's test for multiple comparisons (*$p < 0.05$).

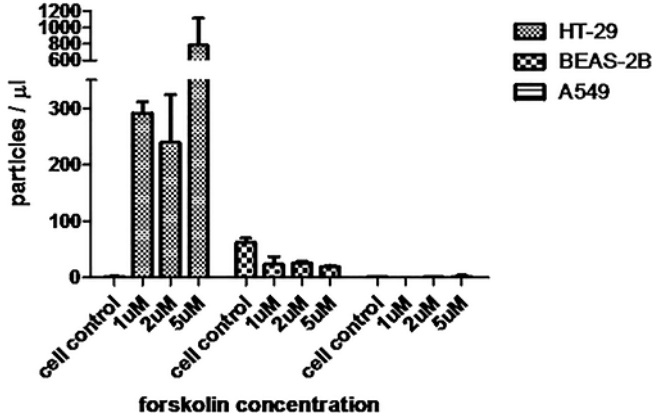

FIG. 7. MP release from HT-29, BEAS-2B, and A549 after forskolin treatment. Cells were cultured on 12-well plate for 24 h. Then, culture supernatant was replaced with 1 mL of media in the presence of forskolin 1, 2, and 5 μM before incubating at 37°C, in 5% CO_2. Culture supernatant was collected at 60 min after incubation. MPs were quantified by flow cytometry. Bar graphs represent the mean ± SEM for three experiments.

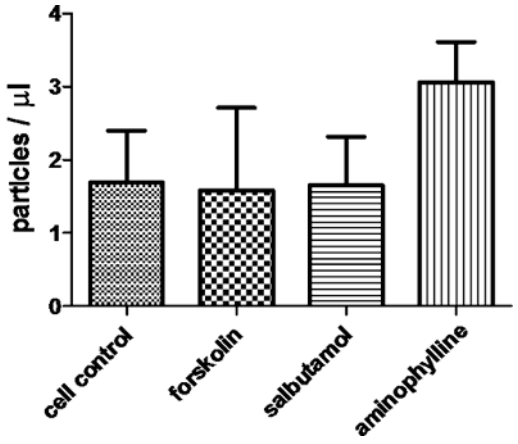

FIG. 8. MP release from A549 after forskolin, salbutamol, and aminophylline treatment. Cells were cultured on 12-well plate for 24 h. Then, culture supernatant was replaced with 1 mL of media in the presence of forskolin, salbutamol, and aminophylline 1, 1, and 10 μM, respectively, before incubating at 37°C, in 5% CO_2. Culture supernatant was collected at 60 min after incubation. MPs were quantified by flow cytometry. Bar graphs represent the mean ± SEM for three experiments.

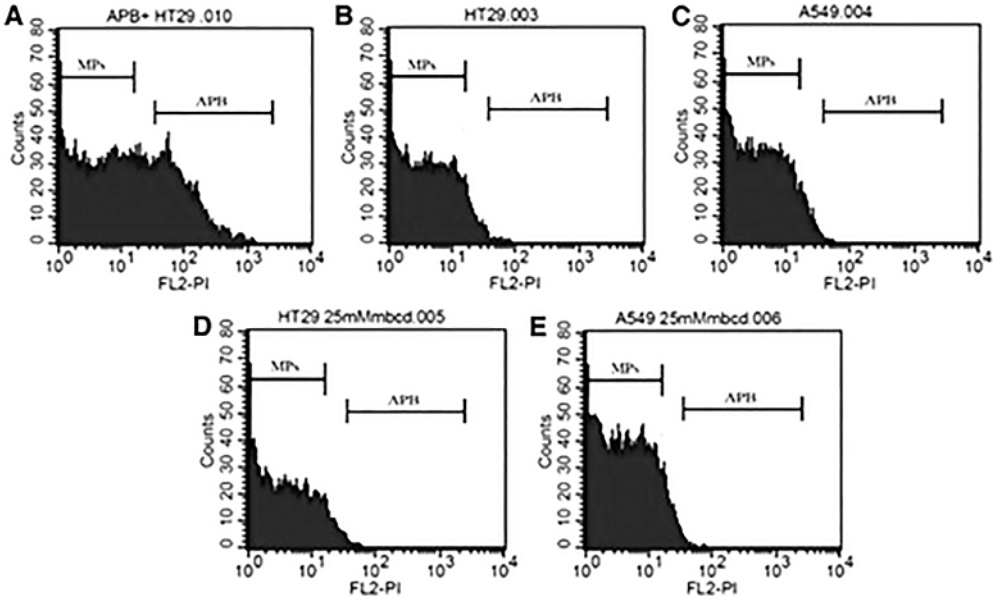

FIG. 9. Verification of MP preparation. To distinguish MPs from apoptotic bodies, the annexin V-positive population of MP samples from A549 and HT-29 cells that culture in normal condition **(B, C)** and treated with MβCD 25 mM for 1 h **(D, E)** was double stained with annexin V and PI. The MP fraction that is defined in gate R2 of Figure 1B was observed to have PI intensity on histogram plot compared with apoptotic bodies from supernatant of hydrogen peroxide-treated HT-29 cells as a positive control **(A)**. PI, propidium iodide.

Table 4. HI Titer Against H1N1 Influenza Virus Strain A/Thailand/MVCU-13/2009 of MP Pellets and Supernatant After 20,000 g Centrifugation

	HT-29		A549	
	MP pellets 20,000 g	**Supernates 20,000 g**	**MP pellets 20,000 g**	**Supernates 20,000 g**
Normal culture condition	Negative	Negative	Negative	Negative
25 mM MβCD treatment				

MP sample obtained from HT-29 and A549 cells that were cultured in normal condition or treated with 25 mM MβCD for 1 h. MβCD, methyl-β-cyclodextrin.

MβCD was the best MP inducer in our experiments. The increase in MP release by MβCD may be related to its ability to remove cholesterol from cellular membranes (18). MβCD has been used in pharmaceutical products for many years because it can interact with drug molecules to form inclusion complexes and modify the drug's properties (26). Thus, administration of drugs containing MβCD through the respiratory tract may enhance innate immunity against influenza infection. It was previously shown that inhalation of aerosolized 75 mM MβCD solutions was nontoxic in mice as assessed by the study of BAL, lung, kidney histology, blood urea, and bronchial responsiveness to methacholine (5). MβCD is also used in nasal formulations of commercial pharmaceutical products (15). However, further *in vivo* investigations are needed to confirm the effect of MβCD on MP induction and innate mucosal defense.

CONCLUSION

MPs were found to be released from various cell lines at various rates. The MPs showed anti-influenza activity, the levels of which could be partially explained by the levels of surface sialic acid. MβCD efficiently activated MP release from some cell lines and might be a candidate for treatment of mucosal viral infection by enhancing innate mucosal defense through MP induction. ■

ACKNOWLEDGMENTS

This study was supported by a research grant from the National Research Council of Thailand. S.J. was supported by Siriraj Graduate Scholarship, Faculty of Medicine Siriraj Hospital, Mahidol University. C.B. was supported by the research assistant program, Faculty of Medicine Siriraj Hospital, Mahidol University, and P.A. was supported by a grant (IRN 60 W0002) from Thailand Research Fund.

COMPLIANCE WITH ETHICAL STANDARDS

Research involving human participants and/or animals: No part of this study was performed with human participants or animals by any of the authors.

AUTHOR DISCLOSURE STATEMENT

The authors declare no conflicts of interest.

REFERENCES

1 Amabile N, Renard JM, Caussin C, et al. Circulating immune complexes do not affect microparticle flow cytometry analysis in acute coronary syndrome. **Blood** 2012;119:2174–2175; author reply 2175–2176. Crossref, Medline, Google Scholar

2 Combes V, Simon AC, Grau GE, et al. In vitro generation of endothelial microparticles and possible prothrombotic activity in patients with lupus anticoagulant. **J Clin Invest** 1999;104:93–102. Crossref, Medline, Google Scholar

3 Connor DE, Exner T, Ma DD, et al. The majority of circulating platelet-derived microparticles fail to bind annexin V, lack phospholipid-dependent procoagulant activity and demonstrate greater expression of glycoprotein Ib. **Thromb Haemost** 2010;103:1044–1052. Crossref, Medline, Google Scholar

4 de Gonzalo-Calvo D, Cenarro A, Civeira F, et al. microRNA expression profile in human coronary smooth muscle cell-derived microparticles is a source of biomarkers. **Clin Invest Arterioscler** 2016;28:167–177. Medline, Google Scholar

5 Evrard B, Bertholet P, Gueders M, et al. Cyclodextrins as a potential carrier in drug nebulization. **J Control Release** 2004;96:403–410. Crossref, Medline, Google Scholar

6 Freyssinet JM, and Toti F. Formation of procoagulant microparticles and properties. **Thromb Res** 2010;125 Suppl 1:S46–S48. Crossref, Medline, Google Scholar

7 Guervilly C, Lacroix R, Forel J-M, et al. High levels of circulating leukocyte microparticles are associated with better outcome in acute respiratory distress syndrome. **Crit Care** 2011;15:R31. Crossref, Medline, Google Scholar

8 Hagerstrand H, Bobrowska-Hagerstrand M, Lillsunde I, et al. Vesiculation induced by amphiphiles and ionophore A23187 in porcine platelets: a transmission electron microscopic study. **Chem Biol Interact** 1996;101:115–126. Crossref, Medline, Google Scholar

9 Huang X, He J, Liu M, et al. The influence of aminophylline on the nanostructure and nanomechanics of T lymphocytes: an AFM study. **Nanoscale Res Lett** 2014;9:518. Crossref, Medline, Google Scholar

10 Iida K, Whitlow MB, and Nussenzweig V. Membrane vesiculation protects erythrocytes from destruction by complement. **J Immunol (Baltimore, MD: 1950)** 1991;147:2638–2642. Medline, Google Scholar

11 Insel PA, and Ostrom RS. Forskolin as a tool for examining adenylyl cyclase expression, regulation, and G protein signaling. **Cell Mol Neurobiol** 2003;23:305–314. Crossref, Medline, Google Scholar

12 Juergens UR, Stober M, Libertus H, et al. Different mechanisms of action of beta2-adrenergic receptor agonists: a comparison of reproterol, fenoterol and salbutamol on monocyte cyclic-AMP and leukotriene B4 production in vitro. **Eur J Med Res** 2004;9:365–370. Medline, Google Scholar

13 Kalra H, Drummen GP, and Mathivanan S. Focus on extracellular vesicles: introducing the next small big thing. **Int J Mol Sci** 2016;17:170. Crossref, Medline, Google Scholar

14 Kesimer M, Scull M, Brighton B, et al. Characterization of exosome-like vesicles released from human tracheobronchial ciliated epithelium: a possible role in innate defense. **FASEB J** 2009;23:1858–1868. Crossref, Medline, Google Scholar

15 Loftsson T, and Brewster ME. Cyclodextrins as functional excipients: methods to enhance complexation efficiency. **J Pharm Sci** 2012;101:3019–3032. Crossref, Medline, Google Scholar

16 Luini A, Lewis D, Guild S, et al. Hormone secretagogues increase cytosolic calcium by increasing cAMP in corticotropin-secreting cells. **Proc Natl Acad Sci U S A** 1985;82:8034–8038. Crossref, Medline, Google Scholar

17 Lusche DF, Bezares-Roder K, Happle K, et al. cAMP controls cytosolic Ca2+ levels in Dictyostelium discoideum. **BMC Cell Biol** 2005;6:12. Crossref, Medline, Google Scholar

18 Mahammad S, and Parmryd I. Cholesterol depletion using methyl-beta-cyclodextrin. **Methods Mol Biol** 2015;1232:91–102. Crossref, Medline, Google Scholar

19 Mause SF, and Weber C. Microparticles: protagonists of a novel communication network for intercellular information exchange. **Circ Res** 2010;107:1047–1057. Crossref, Medline, Google Scholar

20 Maxfield FR, and van Meer G. Cholesterol, the central lipid of mammalian cells. **Curr Opin Cell Biol** 2010;22:422–429. Crossref, Medline, Google Scholar

21 Piccin A, Murphy WG, and Smith OP. Circulating microparticles: pathophysiology and clinical implications. **Blood Rev** 2007;21:157–171. Crossref, Medline, Google Scholar

22 Satta N, Toti F, Feugeas O, et al. Monocyte vesiculation is a possible mechanism for dissemination of membrane-associated procoagulant activities and adhesion molecules after stimulation by lipopolysaccharide. **J Immunol (Baltimore, MD: 1950)** 1994;153:3245–3255. Medline, Google Scholar

23 Shet AS, Aras O, Gupta K, et al. Sickle blood contains tissue factor-positive microparticles derived from endothelial cells and monocytes. **Blood** 2003;102:2678–2683. Crossref, Medline, Google Scholar

24 Smalley DM, Sheman NE, Nelson K, et al. Isolation and identification of potential urinary microparticle biomarkers of bladder cancer. **J Proteome Res** 2008;7:2088–2096. Crossref, Medline, Google Scholar

25 Soekmadji C, Russell PJ, and Nelson CC. Exosomes in prostate cancer: putting together the pieces of a puzzle. **Cancers** 2013;5:1522–1544. Crossref, Medline, Google Scholar

26 Stella VJ, and He Q. Cyclodextrins. **Toxicol Pathol** 2008;36:30–42. Crossref, Medline, Google Scholar

27 Stewart CE, Torr EE, Mohd Jamili NH, et al. Evaluation of differentiated human bronchial epithelial cell culture systems for asthma research. **J Allergy (Cairo)** 2012;2012:943982. Medline, Google Scholar

28 Suptawiwat O, Boonarkart C, Chakritbudsabong W, et al. The N-linked glycosylation site at position 158 on the head of hemagglutinin and the virulence of H5 N1 avian influenza virus in mice. **Arch Virol** 2015;160:409–415. Crossref, Medline, Google Scholar

29 Suptawiwat O, Ruangrung K, Boonarkart C, et al. Microparticle and anti-influenza activity in human respiratory secretion. **PLoS One** 2017;12:e0183717. Crossref, Medline, Google Scholar

30 Tesse A, Martinez MC, Meziani F, et al. Origin and biological significance of shed-membrane microparticles. **Endocr Metab Immune Disord Drug Targets** 2006;6:287–294. Crossref, Medline, Google Scholar

31 Wolf P. The nature and significance of platelet products in human plasma. **Br J Haematol** 1967;13:269–288. Crossref, Medline, Google Scholar

32 Wright DT, Fischer BM, Li C, et al. Oxidant stress stimulates mucin secretion and PLC in airway epithelium via a nitric oxide-dependent mechanism. **Am J Physiol** 1996;271:L854–L861. Medline, Google Scholar

33 Yan R, Wang Z, Yuan Y, et al. Role of cAMP-dependent protein kinase in the regulation of platelet procoagulant activity. **Arch Biochem Biophys** 2009;485:41–48. Crossref, Medline, Google Scholar

34 Zwaal RF, Comfurius P, and Bevers EM. Surface exposure of phosphatidylserine in pathological cells. **Cell Mol Life Sci** 2005;62:971–988. Crossref, Medline, Google Scholar

Serological and T Cell Responses After Varicella Zoster Virus Vaccination in HIV-Positive Patients Undergoing Renal Dialysis

By Elda Righi,[1, 2, *] Alessia Carnelutti,[1] Alessandro La Rosa,[1] Assunta Sartor,[3] Patrizia Tulissi,[4] Tolinda Gallo,[5] Federico Ivaldi,[1, 6,*] and Matteo Bassetti V, [7]

1. Infectious Diseases Division, 3. Microbiology Unit, 4. Nephrology, Dialysis and Transplantation Unit, 5. Public Health Department, Santa Maria della Misericordia University Hospital, Udine, Italy; 2. Department of Diagnostics and Public Health, University of Verona, Verona, Italy; 6. Center of Excellence for Biomedical Research (CEBR), University of Genoa, Genoa, Italy; 7. Department of Medicine, University of Udine, Udine, Italy. *These two authors contributed equally to this paper.

ABSTRACT

Limited data on varicella zoster virus (VZV) vaccine responses are available in HIV-positive adults, especially among those with end-stage renal disease on dialysis or undergoing kidney transplantation (KT). Serological and T cell responses were analyzed using anti-VZV IgG titers, enzyme-linked immunosorbent assay and flow cytometric intracellular cytokine staining (ICS) in two HIV-positive kidney transplant candidates undergoing dialysis and receiving VZV immunization. The results were compared with two HIV-positive and two HIV-negative VZV-seropositive patients (two kidney transplant candidates and two kidney transplant recipients), and with one HIV-negative vaccinee. HIV-positive VZV-susceptible patients received two doses of VZV vaccine 12 weeks apart. No adverse

Sebastian Kaulitzki / Science Photo Library/Getty Images

events were reported. Serological data were indicative of immunological response in one patient and corresponded to T cell responses. The second patient showed only a transient increase in anti-VZV IgG titers, but reported positive $CD4^+$ T cell responses that were maintained after KT. Positive T cell and serological responses were detected in both HIV-positive and HIV-negative controls. VZV vaccination appeared safe and effective in HIV-positive KT candidates. VZV-specific T cell immunity was detected among transplant candidates and after KT. The assessment of VZV-specific T cell immunity using flow cytometric ICS may be more reliable compared to serology in assessing responses to VZV vaccine in this group.

BACKGROUND

Varicella zoster virus (VZV) infection represents a life-threatening disease in immunocompromised patients due to potential visceral complications (20,26). Although virus-specific cellular immunity is considered critical to control viral replication (1), open questions remain on the immunogenicity of the vaccine in immunocompromised hosts (23). In HIV-infected children, VZV immunization showed satisfactory responses, also among subjects with impaired immunity (e.g., $CD4^+$ T cell >15%, absolute count >200 cells/mm^3) (14). Currently, two doses of VZV vaccine 12 weeks apart are suggested in stable HIV-positive patients with CD4 count of at least 200 cells/mm^3 (22). Susceptible dialysis patients, especially if kidney transplantation (KT) is being considered, should receive VZV vaccination due to the high risk of severe posttransplant disease (3,6). Limited data on VZV vaccine responses over time, however, are available in HIV-positive adults undergoing dialysis or KT.

OBJECTIVES

Anti-VZV IgG titers and antigen-specific T cell responses to VZV immunization were analyzed in two HIV-positive KT candidates using enzyme-linked immunosorbent assay (ELISA) and flow cytometric intracellular cytokine staining (ICS) assay. The results were compared with HIV-positive and HIV-negative VZV-seropositive patients (including two kidney transplant candidates and two kidney transplant recipients), and with one HIV-negative vaccinee.

STUDY DESIGN

HIV-positive, VZV-seronegative patients received two doses of live attenuated Oka vaccine (Varivax®, MSD, Italy) 12 weeks apart. Immune responses were analyzed 6 weeks after the first and second dose, 6 months after immunization, and following KT in one patient. Blood was obtained after approval of the local Institutional Ethical Committee, and informed consent was collected from all study participants.

Serological tests were performed using the fully automated Liaison VZV IgG immunoassay (DiaSorin, Vercelli, Italy), based on chemiluminescence technology using partially purified extract of infected cell cultures and calibrated against WHO international preparation (W1044) (15). This assay is routinely used at our institution for assessment of VZV immunity and has shown optimal sensitivity (>97%) and specificity (100%) compared to other commonly used tests in clinical practice (2,19).

The cell-ELISA method has been previously described and was used to quantitate peripheral blood mononuclear cell (PBMC) INF-γ production (16,17). IFN-γ antibody pairs and ELISA kit were obtained from Biolegend (San Diego, CA). Results are shown as the optical density at 405 nm as picograms/milliliter (pg/mL) of cytokine, according to a standard titration curve. Phosphate-buffered saline and RPMI 1640 medium were purchased from BioWhittaker (Verviers, Belgium). RPMI 1640 medium was enriched with 10 mM L-glutamine and 5% fetal calf serum (FCS) to obtain complete medium. Antibodies for phenotyping and intracellular cytokine staining (ICS) were from Becton Dickinson (BD, San Jose', CA). VZV-infected cell lysate (VZV antigen) was purchased from Microbix (Toronto, Canada) and used as a stimulant. Other antigens included *Candida albicans* (Microbix) and the mitogen phytohemagglutinin (PHA) (Sigma-Aldrich, Milan, Italy). Final antigen concentration was 1 μg/mL.

Flow cytometry analysis (BD Biosciences FACSCantoII™) and ICS (Cytofix-Cytoperm, BD) were used to assess T cell subpopulations ($CD3^+CD4^+$ T-helper cells and $CD3^+CD8^+$ effector T cells), and cytokine production (interferon-γ, INF-γ) from nonstimulated (NS, incubated with medium), VZV-stimulated cells, or PBMCs stimulated with phorbol myristate acetate and ionomycin (PMA/IONO) (Sigma-Aldrich) serving as positive control antigen. For ICS, PBMCs (10^6 PBMCs/well) were incubated for 18 h with T cell medium, costimulatory antibodies (αCD28 and αCD3; BD), and antigens (VZV and PMA/IONO). Brefeldin-A (BD Pharmingen) was added for the final 5 h. Cells were permeabilized using the BD-FACS intracellular cytokine staining kit according to the manufacturer's instructions and stained for αCD3-FITC, αCD4–PECy7, and αIFN-γ-PE. $CD3^+CD4^+$ and $CD3^+CD8^+$ lymphocytes were assessed for IFN-γ production. IFN-γ^+ T cells were designated as VZV-specific $CD4^+$ and $CD8^+$ T cells. Data collected on the flow cytometer were compensated and analyzed with FlowJo (Treestar, Ashland, OR).

RESULTS

We have analyzed cell-mediated responses to VZV antigens in four HIV-positive patients, including three KT candidates and one recipient, two HIV-negative VZV-seropositive patients (a kidney transplant candidate and one transplant recipient),

Table 1. Characteristics of Patients Included in the Study

Characteristic	Patient 1	Patient 2	Patient 3	Patient 4	Patient 5	Patient 6	HC
Age (years), sex	37, F	34, F	50, M	38, F	28, M	53, M	34, F
Time on dialysis (years)	4 (pre-KT)	5 (current)	6 (pre-KT)	6 (current)	7 (current)	3 (pre-KT)	–
HIV CDC stage	C3	B3	B1	B3	–	–	–
HIV-RNA cp/mL[a]	UN	UN	UN	UN	–	–	–
CD4 count cell/ mm3 (%)[b]	559 (22)	528 (47)	990 (47)	220 (18)	733 (45)	561 (42)	660 (55)
Timing between VZV vaccine doses	12 weeks	12 weeks	–	–	–	–	12 months
KT performed	Yes	On waiting list	Yes	On waiting list	On waiting list	Yes	–

[a]All patients were stable and receiving antiretroviral treatment.

[b]At the time of the first VZV vaccine dose for immunized patients.

KT, kidney transplantation; HC, healthy control; UN, undetectable HIV viral load; VZV, varicella zoster virus.

and one HIV-negative vaccinee. Patients' characteristics are summarized in Table 1. All four HIV-positive patients were stable and receiving antiretroviral therapy. VZV-seropositive HIV-positive and HIV-negative patients reported a history of prior varicella infection. Two patients (Patient 1 and 2) with no previous history of VZV disease or immunization were found seronegative for VZV during routine pretransplant screening and received two doses of VZV vaccine. Patient 1 underwent KT 8 months after vaccination, while Patient 2 remained on the kidney transplant waiting list. No complications were detected after vaccine administration in both vaccinees, and VZVDNA measurements in blood were persistently negative. Table 2 reports IFN-γ production from PBMCs by cell-ELISA. Positive responses to *Candida* spp. (ranging from 74 to 244 pg/mL) and PHA (positive control) were registered in all subjects. Patient 1 had no detectable IFN-γ production (except for a slight transient increase after the first dose of VZV vaccine), while Patient 2 showed persistent response after the second dose of vaccine. Patients 3 and 4 (HIV-positive controls) and Patients 5 and 6 (HIV-negative controls) showed IFN-γ production to VZV antigen stimulation. The healthy control received two doses of VZV vaccine due to persistent VZV seronegativity. Assessment of cell-mediated immunity showed positivity after the first and second dose of VZV vaccine and weak, but positive response at the

Table 2. Cellular Immune Response Assessed Through Cell-ELISA Measuring IFN-γ Production After Peripheral Blood Mononuclear Cell Stimulation with VZV and Candida spp. Antigens and Phytohemagglutinin (PHA, Mitogen)

IFN-γ (pg/mL)	Before VZV vaccine or baseline	After 1st dose	After 2nd dose	6-month follow-up
Patient 1				
VZV	Negative	31	Negative	Negative[a]
Candida spp.	156	134	146	114
PHA	330	313	217	173
Patient 2				
VZV	Negative	Negative	85	90
Candida spp.	91	74	127	100
PHA	199	249	330	258
Patient 3				
VZV	109			
Candida spp.	140	–	–	–
PHA	332			
Patient 4				
VZV	73			
Candida spp.	127	–	–	–
PHA	288			
Patient 5				
VZV	204			
Candida spp.	244	–	–	–
PHA	433			
Patient 6				
VZV	160			
Candida spp.	189	–	–	–
PHA	373			
Healthy control				
VZV	Negative	31	49	26
Candida spp.	140	151	174	171
PHA	493	434	534	431

[a]Results were confirmed negative 5 months after kidney transplantation.
PHA, phytohemagglutinin.

6-month follow-up. Figure 1 reports VZV-specific cell-mediated immunity assessed by cell-ELISA compared with serological responses, showing substantial correspondence between the two tests. In particular, Patient 1 had only a transient increase of VZV IgG, while Patient 2 showed seroconversion after the second dose of VZV vaccine.

VZV-specific $CD4^+$ and $CD8^+$ T cellular immunity were measured by ICS (Table 3). Patient 1, who did not show response to VZV vaccination at serological and cell-ELISA tests, showed a higher percentage of $CD3^+CD4^+IFN\text{-}\gamma^+$ in VZV-stimulated compared to nonstimulated cells after the second dose of VZV vaccine, at the 6-month follow-up and 5 months after KT (Fig. 2A). Figure 2B and C show that VZV-specific $CD4^+$ T cell response was also documented among HIV-positive and HIV-negative kidney transplant recipients (Patient 4, Fig. 2B, and Patient 6, Fig. 2C). Similarly reactivity to PMA/IONO (positive control) was reported

Table 3 shows that VZV-specific $CD4^+$ and $CD8^+$ T cell responses were reported by HIV-positive and HIV-negative controls. Although VZV-specific $CD8^+$ T cell immunity was detected in Patient 1 and 2, net responses were lower compared with $CD4^+$ T cell responses.

The healthy vaccinee displayed VZV-specific T cell responses after vaccination with reduction of IFN-γ production over time, especially for $CD8^+$ T cells (Table 3).

DISCUSSION

The widespread introduction of VZV vaccination has disclosed the presence of nonresponders or the loss of humoral immunity, even among healthy subjects (21). These conditions can be challenging for clinicians facing the potential threat of VZV susceptibility in high-risk subjects. In this context, the reliability of VZV serological response has been questioned (7). Although a positive IgG titer remains the "gold standard" for assessing VZV protection, VZV antibodies represent only a surrogate of the correlate of protection (7). Immunological studies report that while VZV antibodies can fade after vaccination, VZV-specific $CD4^+$ cell response is a more reliable correlate of protection (13,18). Data supporting this hypothesis, however, are limited. A case report analyzing T cell responses in a vaccinated subject with undetectable VZV antibodies after serological reconversion showed persistently positive CD4-mediated immunity (18). In another report, a healthy subject with absence of VZV antibody titer after three doses of vaccine showed positive cellular responses measured by ICS and, despite documented contacts with infectious subjects, did not develop VZV disease (2). In our study, we observed persistent VZV-specific $CD4^+$ T cell responses in an HIV-positive KT recipient vaccinee with only transient serological responses and CD4 count >500 cells/mm^3. Other reports highlight that CD4 count and HIV-RNA may not be critical in predicting VZV-specific immunity (2,25). In our study,

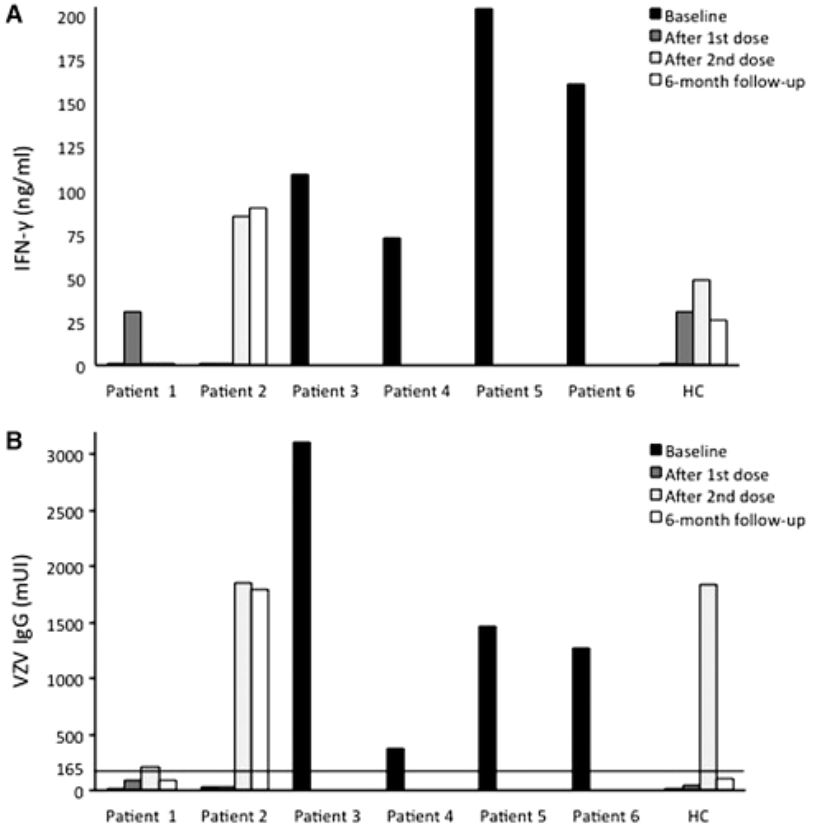

FIG. 1. Comparison of immune responses measured by PBMC IFN-γ production by cell-ELISA and serological responses (IgG positivity) in HIV-positive patients and controls. (A) Cell-mediated immunity measured by PBMC IFN-γ production (ng/mL) by cell-ELISA among HIV-positive VZV vaccinee (Patient 1 and 2), HIV-positive VZV-seropositive patients (Patient 3 and 4), HIV-negative VZV-seropositive dialysis patient and kidney transplant recipient (Patient 5 and 6), and HC. Patient 1 showed only a transient response to vaccination (B) Humoral immunity measured by IgG positivity (positive results >165 mUI). ELISA, enzyme-linked immunosorbent assay; HC, healthy control; PBMC, peripheral blood mononuclear cell; VZV, varicella zoster virus.

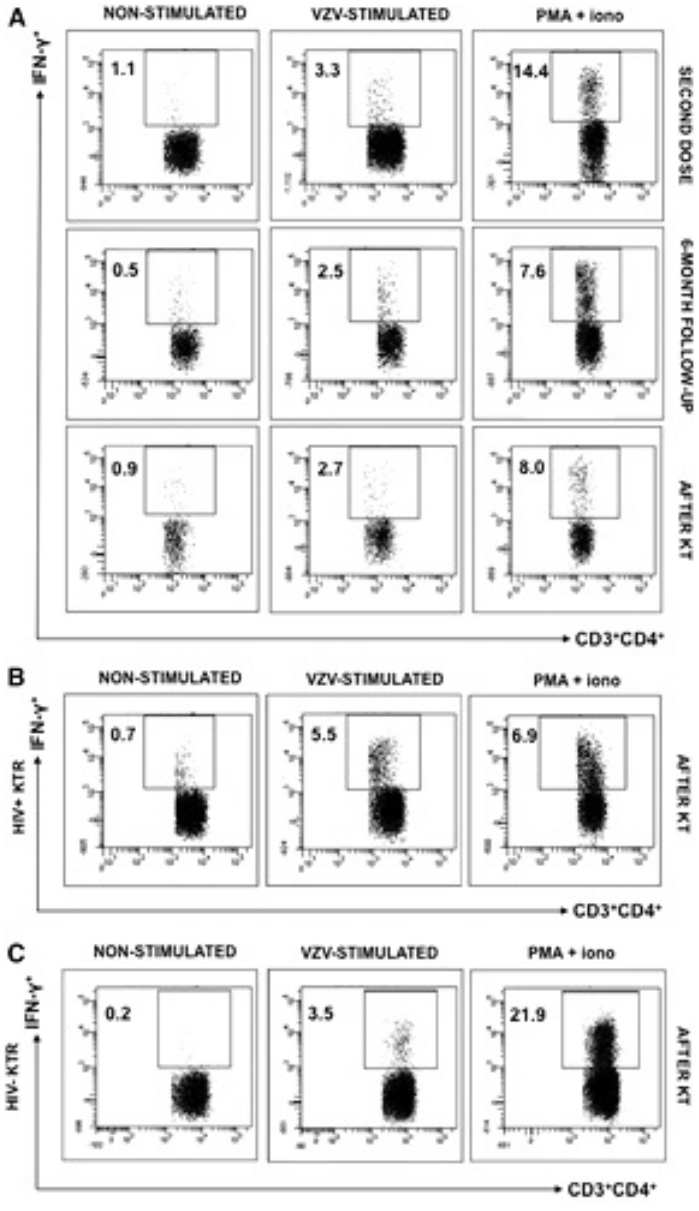

FIG. 2. Representative dot plots showing the frequency of IFN-γ positive events in CD3+CD4+ T cells by intracellular cytokine staining in kidney transplant patients. Patient 1 (HIV-positive kidney transplant recipient vaccinee) postvaccine samples (A), Patient 4 (HIV-positive, VZV-seropositive kidney transplant recipient) (B), Patient 6 (HIV-negative, VZV-seropositive kidney transplant recipient) (C). PBMCs were stained with anti-CD3, anti-CD4, and anti-IFN-γ. (A) Higher percentage of CD3+CD4+IFN-γ+ was shown for VZV-stimulated compared to NS cells for the HIV-positive patient at different time points (after the second vaccine dose, at 6-month follow-up, and 5 months after kidney transplantation). (B) Higher percentage of CD3+CD4+IFN-γ+ was shown for VZV-stimulated compared to nonstimulated cells for the HIV-positive, VZV-seropositive (previous infection, natural protection) patient. (C) Higher percentage of CD3+CD4+IFN-γ+ was shown for VZV-stimulated compared to nonstimulated cells for the HIV-negative, VZV-seropositive (previous infection, natural protection) patient. PMA + ionomycin-stimulated cells were considered positive controls. A total of 250,000 events were collected. NS, nonstimulated; PMA, phorbol-myristate-acetate.

we detected preserved cellular immunity toward other antigens (e.g., *Candida* spp. and mitogens) that did not correlate with patients' CD4 cell count. A study involving 67 HIV-positive subjects with T CD4 ≥ 400 cells/mm^3 demonstrated that the vaccine was safe, but only modestly immunogenic for HIV-positive subjects compared to HIV-negative vaccinees using lymphocyte proliferation assays and IFN-γ ELISPOT (26).

A factor that may explain the variability in the immunological results to VZV vaccination is the different sensitivity shown not only by commercial serological VZV tests (9,21) but also across cellular immunity assays (4). Cell-ELISA has previously demonstrated to be a reliable test for assessing antigen responses in HIV-positive patients (16,17), although VZV responses were not specifically investigated. A previous report analyzing VZV-specific T cell responses after zoster vaccination found comparable data using ELISPOT and ICS (12). The flow cytometric ICS assay, in particular, is one of the primary tests for the analysis

Table 3. VZV-Specific CD4+ and CD8+ T Cell Immune Response Assessed Through Flow Cytometry Measuring IFN-γ Production After Peripheral Blood Mononuclear Cell Stimulation with VZV Antigens and Phytohemagglutinin (PHA, Mitogen)

	Before VZV vaccine or baseline		After VZV vaccinea		6-month follow-up		After KT	
IFN-γ (%)	CD4	CD8	CD4	CD8	CD4	CD8	CD4	CD8
Patient 1								
Unstimulated	0.5	1.1	1.1	0.7	0.5	1.1	0.9	0.2
VZV	0.5	1.2	3.3	7.9	2.5	1.3	2.7	2.4
PHA	7.6	5.9	14.4	19.5	7.6	5.9	8.0	8.2
Patient 2								
Unstimulated	1.3	1.2	0.7	1.4	0.6	1.0		
VZV	1.2	1.2	2.7	1.7	1.4	1.8		–
PHA	10.3	24.0	8	22.0	12.2	10.0		
Patient 3								
Unstimulated							0.7	1.1
VZV	–	–	–	–	–	–	5.5	6.9
PHA							6.9	10.4
Patient 4								
Unstimulated	0.6	1.7						
VZV	1.5	2.4	–	–	–	–		
PHA	10.7	10.4						
Patient 5								
Unstimulated	0.1	1.1						
VZV	5.9	12.4	–	–	–	–		
PHA	23.1	16.6						
Patient 6								
Unstimulated							0.2	0.6
VZV	–	–	–	–	–	–	3.5	5.5
PHA							21.9	14.9
Healthy control								
Unstimulated	0.8	1.2	0.2	1.1	0.5	1.0		
VZV	0.7	1.0	1.8	2.2	0.9	1.1		
PHA	4.9	3.8	3.8	3.6	6.7	3.8		

[a] Measured after the second dose of VZV vaccine.

of vaccine-induced T cells in clinical trials (8). ICS has demonstrated to be useful in measuring antigen-specific responses in HIV-positive subjects, potentially explaining Patient 1 positivity compared to cell-ELISA (3). We also observed that antigen-specific (VZV, Candida, and mitogen related) T cell responses remained preserved among HIV-positive patients after KT and were comparable with those detected in the HIV-negative kidney transplant recipient. Despite VZV-specific $CD4^+$ T cell immunity being detected in the HIV-positive kidney transplant vaccinee, we opted to maintain the patient on VZV prophylaxis with valaciclovir due to the profound immunosuppression associated with the early posttransplant period.

Our study has several limitations. First, IgG titers were assessed using a fully automated system instead of other reference tests assessing glycoprotein-specific antibodies (e.g., fluorescent-antibody to-membrane-antigen test,

FAMA) or neutralizing antibodies (10,11) that are not used in clinical practice due to the increased complexity and subjectivity in the interpretation of the results. Similar to other reference tests, however, the automated chemiluminescence assay has shown high sensitivity and specificity in detecting protection against clinical varicella (2,19). Second, VZV lysates were chosen as stimulating antigens instead of selected peptide pools. Although VZV lysates have been successful in determining T cell responses through ICC (24), their use may have limited the detection of VZV-specific $CD8^+$ responses compared to $CD4^+$ T cell responses (5). Finally, our results need to be validated in a larger number of vaccinated subjects and at different time points after KT. Nevertheless, the restricted number of adult subjects on dialysis or transplant waiting list requiring VZV immunization represents an intrinsic limitation for these types of studies.

In conclusion, VZV vaccination appeared safe and effective in HIV-positive KT candidates. In one patient, serological and cellular immune responses to VZV appeared suboptimal, although persistent VZV-specific $CD4^+$ T cell responses were detected using ICS and confirmed among transplanted and nontransplanted controls.

Our report highlights the importance of investigating cell-mediated immune responses to VZV vaccination in specific patient populations. While VZV-specific T cells are known to be essential to prevent VZV disease, valid options to avoid life-threatening infections in patients with impaired cellular immunity are limited. Further data on the utility and the most reliable methods to assess VZV-specific immunity, especially among patients with absent serological response and in the clinical setting of HIV infection, are needed to help identify populations for whom interventions, such as VZV prophylaxis, may be beneficial. ■

AUTHOR DISCLOSURE STATEMENT

The authors have no conflict of interests.

REFERENCES

1 Arvin A. Varicella-zoster virus. **Clin Microbiol Rev** 1996;9:361–381. Crossref, Medline, Google Scholar

2 Bender Ignacio RA, Ramchandani MS, Laing KJ, Johnston CM, and Koelle DM. T cell immunity to Varicella-Zoster Virus in the setting of advanced HIV and multiple Varicella-Zoster Virus recurrences. **Viral Immunol** 2017;30:77–80. Link, Google Scholar

3 Chi C, Patel P, Pilishvili T, et al. Guidelines for vaccinating kidney dialysis patients and with chronic kidney disease. Summarized from Recommendations of the Advisory Committee on Immunization Practices (ACIP), CDC 2012. Available at www.cdc.gov/dialysis (Accessed July 12, 2018). Google Scholar

4 De Rosa SC. Vaccine applications of flow cytometry. **Methods** 2012;57:383–391. Crossref, Medline, Google Scholar

5 Dunn HS, Haney DJ, et al. Dynamics of CD4 and CD8 T cell responses to cytomegalovirus in healthy human donors. **J Infect Dis** 2002;186:15–22. Crossref, Medline, Google Scholar

6 Geel A, Zuidema W, van Gelder T, van Doornum G, and Weimar W. Successful vaccination against varicella zoster virus prior to kidney transplantation. **Transplant Proc** 2005;37:952–953. Crossref, Medline, Google Scholar

7 Heininger U, and Seward JF. Varicella. **Lancet** 2006;368:1365–1376. Crossref, Medline, Google Scholar

8 Karlsson AC, Martin JN, Younger SR, et al. Comparison of the ELISPOT and cytokine flow cytometry assays for the enumeration of antigen-specific T cells. **J Immunol Methods** 2003;283:141–153. Crossref, Medline, Google Scholar

9 Katial RK, Ratto-Kim S, Sitz KV, Moriarity R, and Engler RJ. Varicella immunity: persistent serologic non-response to immunization. **Ann Allergy Asthma Immunol** 1999;82:431–434. Crossref, Medline, Google Scholar

10 Krah DL. Assays for antibodies to varicella-zoster virus. **Infect Dis Clin North Am** 1996;10:507–527. Crossref, Medline, Google Scholar

11 Krah DL, Cho I, Schofield T, and Ellis RW. Comparison of gp ELISA and neutralizing antibody responses to Oka/Merck live varicella vaccine (Varivax) in children and adults. **Vaccine** 1997;15:61–64. Crossref, Medline, Google Scholar

12 Laing KJ, Russell RM, Dong L, et al. Zoster vaccination increases the breadth of CD4+ T cells responsive to varicella zoster virus. **J Infect Dis** 2015;212:1022–1031. Crossref, Medline, Google Scholar

13 La Russa P, Steinberg S, and Gershon AA. Varicella vaccine for immunocompromised children: results of collaborative studies in the United States and Canada. **J Infect Dis** 1996;174:S320–S323. Crossref, Medline, Google Scholar

14 Levin MJ, Gershon AA, Weinberg A, et al. Administration of live varicella vaccine to HIV-infected children with current or past significant depression of CD4(+) T cells. **J Infect Dis** 2006;194:247–255. Crossref, Medline, Google Scholar

15 LIAISON VZV-IgG assay, DiaSorin. Available at www.diasorin.com/sites/default/files/allegati_prodotti/vzv_flyer_rev_03.pdf, accessed July 28, 2018. Google Scholar

16 Li Pira G, Ivaldi F, Dentone C, et al. Evaluation of antigen-specific T-cell responses with a miniaturized and automated method. **Clin Vaccine Immunol** 2008;15:1811–1818. Crossref, Medline, Google Scholar

17 Li Pira G, Ivaldi F, Starc N, et al. Miniaturized and high-throughput assays for analysis of T-cell immunity specific for opportunistic pathogens and HIV. **Clin Vaccine Immunol** 2014;21:488–495. Crossref, Medline, Google Scholar

18 Ludwig B, Kraus FB, Allwinn R, et al. Loss of varicella zoster virus antibodies despite detectable cell mediated immunity after vaccination. **Infection** 2006;34:222–226. Crossref, Medline, Google Scholar

19 Maple PA, Rathod P, Smit E, et al. Comparison of the performance of the LIAISON VZV-IgG and VIDAS automated enzyme linked fluorescent immunoassays with reference to a VZV-IgG time-resolved fluorescence immunoassay and implications of choice of cut-off for LIAISON assay. **J Clin Virol** 2009;44:9–14. Crossref, Medline, Google Scholar

20 Perronne C, Lazanas M, Leport C, et al. Varicella in patients infected with the human immunodeficiency virus. **Arch Dermatol** 1990;126:1033–1036. Crossref, Medline, Google Scholar

21 Plotkin SA. Correlates of vaccine-induced immunity. **Clin Infect Dis** 2008;47:401–409. Crossref, Medline, Google Scholar

22 Rubin LG, Levin MJ, Ljungman P, et al. 2013 IDSA clinical practice guideline for vaccination of the immunocompromised host. **Clin Infect Dis** 2014;58:309–318. Crossref, Medline, Google Scholar

23 Sarkadi J. Varicella-zoster virus vaccine, successes and difficulties. **Acta Microbiol Immunol Hung** 2013;60:379–396. Crossref, Medline, Google Scholar

24 Vossen MT, Gent MR, Peters KM, et al. Persistent detection of varicella-zoster virus DNA in a previously healthy child after severe chickenpox. **J Clin Microbiol** 2005;43:5614–5621. Crossref, Medline, Google Scholar

25 Weinberg A, Levin MJ, and Macgregor RR. Safety and immunogenicity of a live attenuated varicella vaccine in VZV-seropositive HIV-infected adults. **Hum Vaccin** 2010;6:318–321. Crossref, Medline, Google Scholar

26 Wiegering V, Schick J, Beer M, et al. Varicella-zoster virus infections in immunocompromised patients—a single centre 6-years analysis. **BMC Pediatr** 2011;11:31. Crossref, Medline, Google Scholar

A Kinase Inhibitor Phenotypic Screen Using a Novel Multiplex T Cell Activation Assay

Zhaoping Liu, Andrea Gomez-Donart and John O'Rourke

Essen Bioscience, Inc., formerly IntelliCyt Corporation, Part of the Sartorius Group, Albuquerque, NM 87111, USA

INTRODUCTION

T cells play a critical role in adaptive immune responses including pathogen elimination and tumor immunosurveillance. The binding of the T cell receptor (TCR) to peptides complexed with major histocompatibility complex (MHC) on antigen presenting cells, along with engagement of co-receptors such as CD4 or CD8 and co-stimulatory molecules (i.e. CD28), triggers an intricate signaling mechanism. TCR signal initiation is mediated by cytosolic tyrosine kinases such as LCK and ZAP70, leading to signal amplification through a network of serine-threonine kinases.1, 2 Activation of the TCR pathway in naive and effector T cells leads to T cell activation, proliferation, and cytokine production.

Modulating TCR engagement and signaling pathway using biologics, small molecules or genetic engineering is highly relevant to many therapeutic areas including cancer immunotherapy, adoptive cell therapy, and vaccine

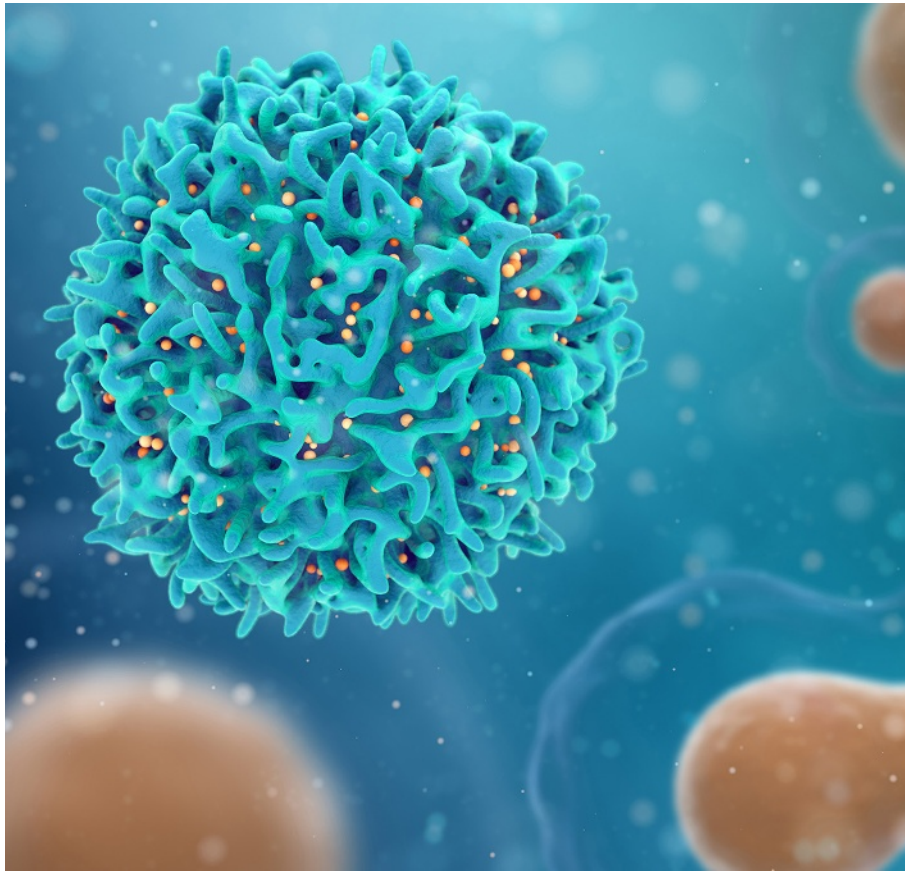

K_E_N / iStock/Getty Images Plus

development. Perturbations leading to increased hyper responsive TCR signaling and enhanced T cell activation is a major cause of autoimmune disease. Genetic defects, mutations and other mechanisms resulting in increased T cell kinase activity are involved in many autoimmune pathologies making them attractive targets for the direct inhibition of T cell activation.(3, 4)

Currently there are 37 FDA approved Kinase Inhibitors (KI), mostly for oncology indications, with approximately 250 in clinical testing.(5) KI drugs specifically targeting early signaling events during T cell activation are a new focus for the treatment of autoimmune diseases with recent FDA approvals for KIs in treating rheumatoid arthritis.(6)

The development of drugs and therapies regulating TCR activity require assays to profile T cell function and health. To address the need for rapid monitoring of T cell function, we developed an optimized, high-content, multiplexed assay using high throughput flow cytometry to measure T cell activation. The Intellicyt® Human T Cell Activation Cell and Cytokine Profiling Kit (TCA Kit) collapses the traditional workflow by evaluating cell phenotype, T cell activation markers, cell proliferation, cell viability, and quantitates secreted cytokines in a single assay using a 96 or 384-well plate format.

In recent years, there has been renewed interest in using phenotypic screens for drug discovery. This screening methodology does not require a specific drug target or knowledge of its role in the pathology of disease, but uses a specific, relevant biological model or signaling pathway to identify appropriate hits.(7) Phenotypic screens are being used with novel compound libraries as wells as drug repurposing and chemogenomic libraries.(8, 9) The use of these known libraries allow for signature and phenotypic matching where the characteristic of a drug with desirable properties can be matched to another drug with an unknown clinical profile.

To illustrate the value of the Intellicyt platform for T cell function in phenotypic screening, we used the TCA Kit to screen a 152 small molecule library of KI for their ability to inhibit human primary T cell activation in peripheral blood mononuclear cells (PBMCs) stimulated with anti CD3/CD28 beads. Samples were acquired on the iQue® advanced flow cytometry platform and the early/late activation markers CD69, CD25 and HLA-DR, and cell proliferation were assessed in viable CD4 and CD8 lymphocytes. To assess T cell function, the levels of secreted IFN-g and TNF-a were quantitated. Data was analyzed and heat maps, IC_{50} curves and cytokine quantitation was generated using the integrated Forecyt software. Profile maps, a unique analysis tool of Forecyt software, was used to integrate assay metrics with Boolean logic to quickly locate hits using defined multiplexed criteria. This application note

demonstrates the insight provided by the use of Intellicyt platform for phenotypic screening of small molecules affecting T cell activation.

MATERIALS

Cells and Reagents

Cryopreserved PBMCs from healthy donors (Astarte Biologicals) were cultured in PBMC media (RPMI 1640, supplemented with 10% fetal bovine serum, 10 ng/mL of human IL-2, non-essential amino acids, sodium pyruvate and penicillin-streptomycin (all purchased through VWR)). CD3/CD28 DynaBeads (ThermoFisher Scientific), phytohemagglutinin (PHA, Sigma) and enterotoxin type B from Staphylococcus aureus (SEB, List Biological Laboratories) were used for T cell activation. The 152 compound chemogenomic KI library was purchased from Cayman Chemicals. T cell activation was assessed using the Intellicyt Human T Cell Activation Cell and Cytokine Profiling Kit, which measures cell proliferation and viability, cell surface early/late activation markers (CD69, CD25 and HLA-DR) and secreted cytokines (IFN-g and TNF-a).

METHODS

Profiling T Cell Activation

For proof of concept (POC) studies to test assay robustness, PBMCs from a single donor were cultured in a 96-well plate at a final concentration of 106 cells/ml. Different activation reagents (DynaBeads, PHA, and SEB) were added to the cells using an 11 point, 2-fold dilution series and each series was done in duplicate wells. Media without activation compounds were used as a control. T cell activation was measured by the TCA kit from a 10 μl cell/supernatant mixture sample transferred to the assay well from each culture well at 1, 3 and 6 days post-stimulation. Data were acquired on the iQue platform and analyzed with Forecyt software using the T cell activation kit data template (See data acquisition section below).

T Cell Activation Kinase Inhibitor Screening and Dose Response Assays

Cryopreserved PBMCs were cultured overnight in PBMC media. Cells were cultured in a 96-well plate in PBMC media with 20 μM of the indicated KI for 1 hour and stimulated with CD3/CD28 DynaBeads for 24 hours. The final concentration of cells were 106 cells/ml with a final concentration of 10 μM for the KI and a final culture volume of 100 μl. Negative controls were cells cultured without any drug, and positive assay control were cells cultured with 10 μM of the phosphatase inhibitor Cyclosporine A, a known inhibitor of T cell activation.

Twenty-four hours later, T cell activation was assessed following the TCA kit protocol. Briefly, INF-g and TNF-a standard curves were generated in a separate standard-alone

plate, and 10 μl of each sample culture from each well of the original 2 culture plates were transferred to 2, 96-well assay plates. Sequential addition of cytokine beads and cytokine detection antibodies were followed by a cocktail of viability dye and fluorescent CD antibodies. The total assay time was approximately 4 hours.

Dose response studies were performed on select KI using the same basic protocol as the initial kinase screening assay. An 11 point, 2-fold serial dilution was used for each kinase inhibitor with a concentration range of 10 μM to 10 nM. Media only was used for each compound as a negative control for the study.

Data Acquisition and Analysis

Samples were acquired on the iQue advanced flow cytometry platform. The panel design of the TCA kit dictated the violet, blue and red (VBR) laser configuration. The acquisition protocol and data analysis, including event gates and gating strategy, activation metrics, heat maps, standard curves and IC/EC 50 curves were auto-generated using the TCA template and Forecyt software. Standard curves to quantitate the levels of secreted IFN-g and TNF-a were generated using a 4-parameter curve fit with 1/Y2 weighting factor. The linear range for each standard curve was calculated using Forecyt software. Profile maps were created in the multi-plate analysis Panorama feature in the Forecyt software. Profile maps were used to identify compound hits with specific criteria, including inhibition of all activation metrics and select markers.

RESULTS AND DISCUSSION

The discovery and development of small molecules and antibodies targeting T cell function, as well as T cell-based cell therapies and cell manufacturing, require assays to rapidly and reliably profile T cell activation and cell health. To address this need, Intellicyt developed the TCA Kit to rapidly deliver high-content T cell activation data. Figure 1 shows the assay biochemistry. The assay discriminates between live and dead cells by using a membrane integrity dye, which stains only dead cells by DNA intercalation. Viable T cell subsets are identified using CD3, CD4 and CD8 antibodies and the cell surface activation markers measure early activation (CD69+), late activation (CD25+) and even later activation (HLA-DR+) in the different T cell subpopulations. The levels of secreted IFN-g and TNF-a are quantitated in the same sample well using a bead-based assay. For long-term studies, cells are stained using proliferation dye (provided in the TCA kit) prior to culture to quantitate cell division during the study time course.

For POC studies, cryopreserved PBMCs from a single donor were cultured for 24 hours and then stained with the Cell Proliferation and Encoder Dye B/Green (included in the TCA Kit). Cells were stimulated with three different well-characterized

T cell activators (CD3/28 DynaBeads, phytohemagglutinin (PHA), or Staphylococcal enterotoxin B (SEB)) using a 12 point, 2-fold serial dilution series (SEB used a 4-fold serial dilution). A 12 point, 3-fold standard curve to quantitate the levels of secreted INF-g and TNF-a were generated. The plate set-up, concentration of cytokine standards, and concentration range of T cell activators are shown in Figure 1.

To perform the assay, 10 μL of sample containing cells and supernatant were transferred from the culture plate to an assay plate on days 1, 3 and 6 after stimulation, and analyzed using the TCA Kit. The data were acquired on the iQue VBR. The time-to-results for the assay, including data acquisition and analysis, is approximately 4 hours. The assay workflow is shown in Figure 2A. The gates and gating strategy are shown in Figure 2B. To increase the ease of use, all gates are pre-drawn, data metrics and visualizations are auto-generated, and color compensation is not required when using the TCA kit template. The seven decade dynamic range of the iQue platform allows for easy discrimination between cytokine capture beads and

FIG.1. Assay Biochemistry and Proof of Concept Study Plate Set-up. The different T cell identifiers, and phenotypic and functional activation markers, measured in each well are seen in the left panel. A typical assay plate set-up used for POC studies is seen in the right panel. This plate includes the standard curves for cytokine quantitation and positive and negative controls.

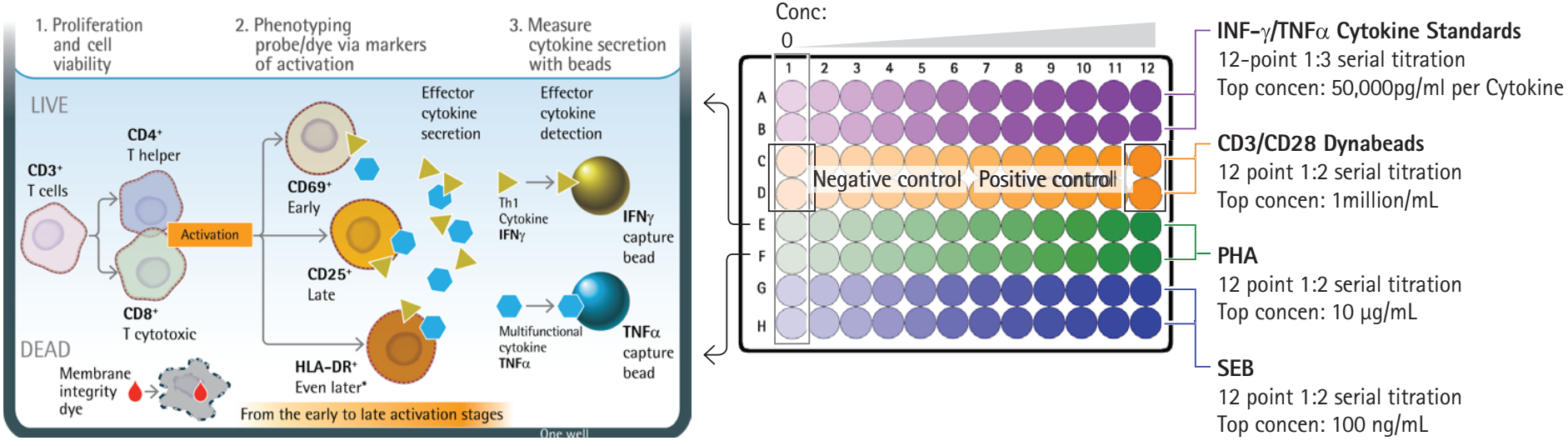

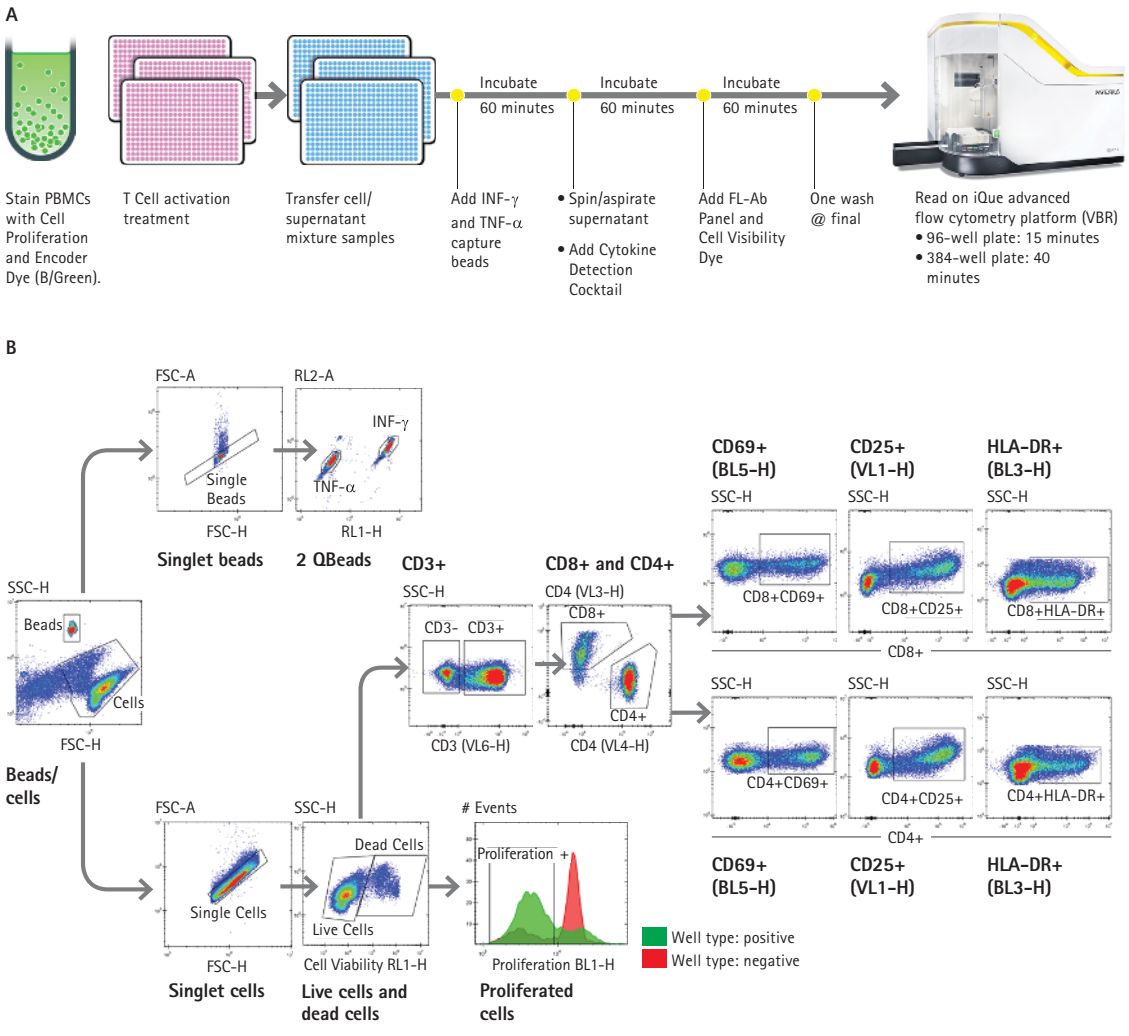

cells using basic forward and side scatter plots. Due to differences in the capture bead's intrinsic fluorescence, the single cytokine capture beads are resolved into INF-g and TNF-a populations for quantification. For the cell gates, viable single cells are determined, T cell subsets are identified and activation markers are assessed. Cells that proliferated during the experimental time course are identified by a decrease in fluorescent intensity.

The T cell time course activation data were analyzed and line graphs from the POC studies generated using the multi-plate Panorama feature in the Forecyt software. Figure 3 shows cytokine secretion (pg/ml), proliferation (% of CD8+ proliferating cells) and phenotypic activation markers (% of CD8+ cells expressing the indicated

FIG. 2. TCA Assay Workflow and Gating Strategy. A) To perform the TCA assay an aliquot of cells/supernatant mixture (10 μl or 5 μl for 96 or 384-well plate respectively) is transferred to an assay plate. Sequential additions of the pre-mixed reagents are added followed by a final wash before sample acquisition on the iQue advanced flow cytometry platform. B) The gating strategy is included in the TCA template that comes with the kit. Cells and cytokine capture beads are initially separated based on size and granularity. Cytokines capture beads are then resolved while viable cells are determined and T cell subsets and activation status for each subset is assessed.

markers) for each of the three T cell activation reagents with the blue line, red line and green line representing 1, 3 and 6 day post stimulation respectively. The x-axis shows the dose response for each compound. The data show a temporal and dose response for the various activation metrics with differences observed between the three compounds. For example, TNF-a secretion peaks at day 3 with DynaBeads and SEB treatment and significantly decreases at day 6, whereas little temporal difference in TNF-a secretion is observed with cells cultured in PHA. Further analysis show differences in multiple metrics in cells treated with SEB compared to other activating compounds. Taken together, these data show how the TCA Kit can rapidly generate high content data that can identify different mechanisms of action (MOA).

For the initial KI library screen, PBMCs were cultured in IL-2 containing media and treated for 1 hour with 20 μM of each

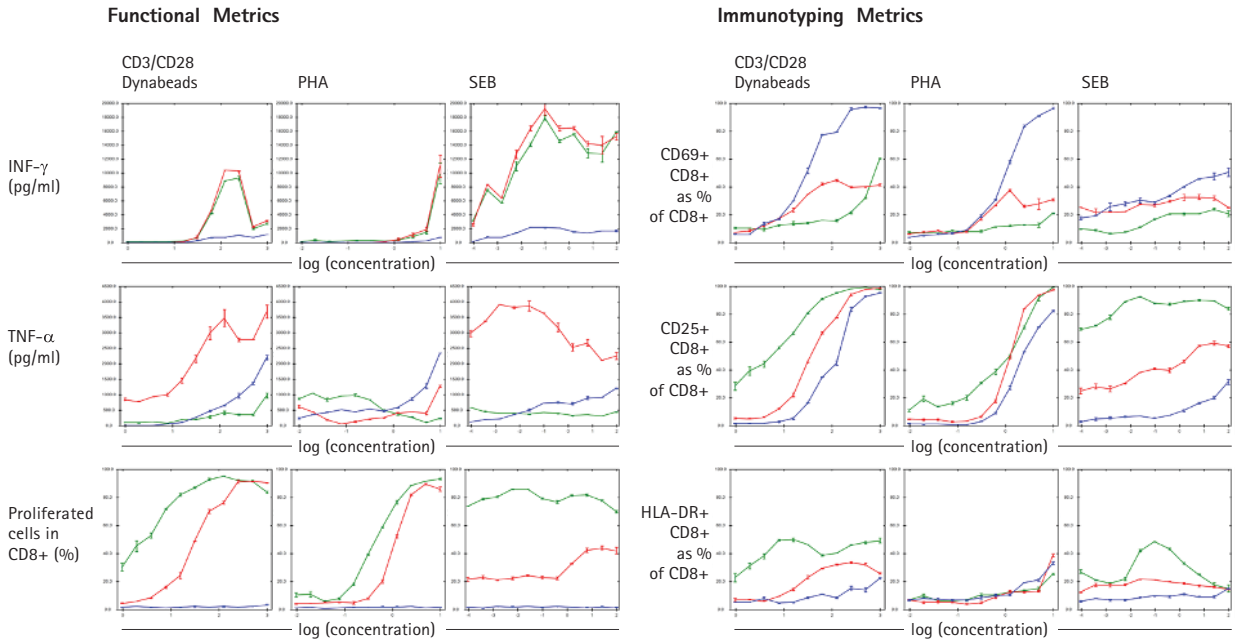

Fig. 3. Selected T cell Activation Data. Line graphs showing the amount of cytokine secretion, % of proliferating CD8+ cells and the % of CD8+ cells co-expressing the various activation markers were generated in Forecyt software. The blue, red and green lines represent 1, 3 or 6 days post stimulation respectively. The x-axis shows increase compound dose (PHA and SEB) or number of DynaBeads per cell. The error bars represent the standard deviation of duplicate measurements. This is representative of an experiment done multiple times.

inhibitor and then cells were activated using anti-CD3/CD28 beads (Figure 4). Twenty-four hours later, the TCA assay was performed and samples were acquired on the iQue VBR. For each of the 2 culture plates, a series of negative controls (media only) were used to determine T cell activation metrics in the absence of compound treatment. For positive controls, cells were treated with 10 μM of cyclosporine A, a known inhibitor of T cell activation (10).

A plate-level analysis showing the percentage of viable CD4 T cells that express the early activation marker CD69 from plate 1 is found in Figure 5. Using this visualization tool, we can quickly identify compounds that have inhibited expression of CD69 (CD69+ cells are in the rectangular gate) as well as KI that drastically reduced CD4+ T cell viability (wells with no cells, i.e. well H2). Below, in the plate-level view, are examples of inhibitors that affect different kinase families. In wells containing media alone,

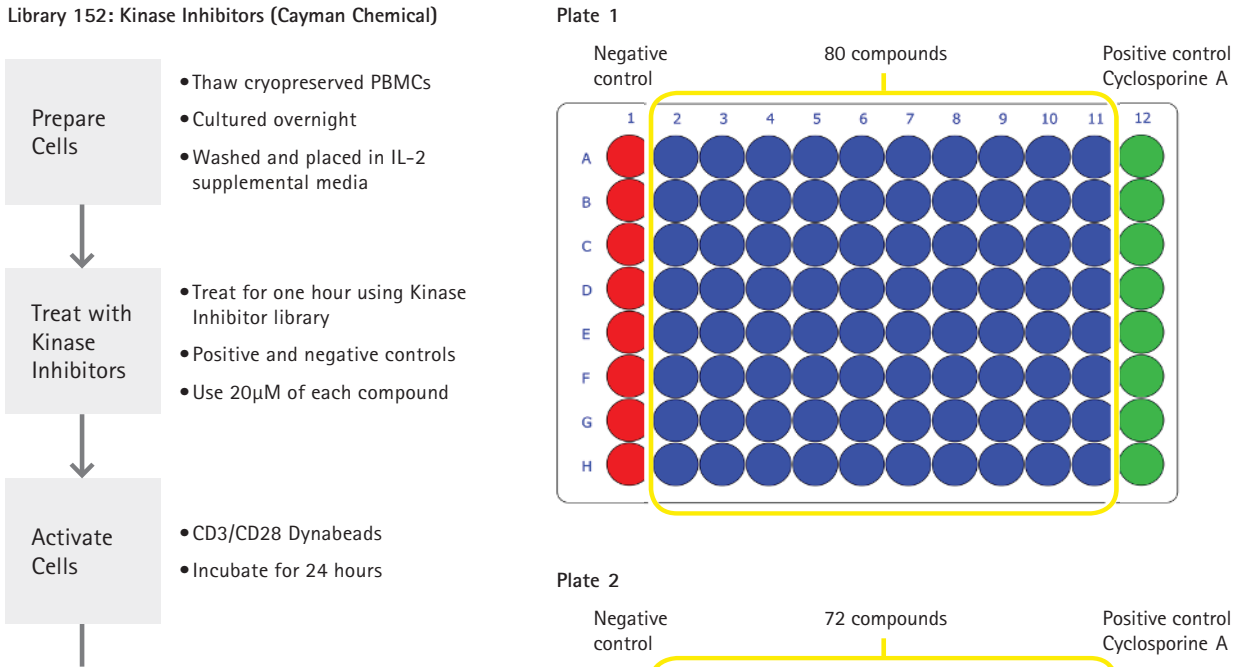

FIG. 4. Kinase inhibitor screening experimental setup. PBMCs were cultured overnight and added to wells containing individual KI (final concentration of 20μM). One hour later, anti CD3/CD28 DynaBeads were added to each culture to activate T cells and TCA assay was performed 24 hours later.

86% of the CD4 cells are activated as assessed by CD69 expression and treatment with the FDA-approved Jak 1/2 inhibitor Ruxolitinib which reduced the percentage of CD4+CD69+ cells down to 55%. The Src inhibitor PP2 dramatically inhibited CD69 expression as only 3% of the CD4 T cells expressed CD69. Other compounds showed a range of CD69 inhibition.

In Figure 5, we show a single activation metric (CD69) in the T-helper subset, whereas the TCA kit generated 15 different parameters requiring integration to provide a more complete and insightful picture of the role that different KI have in T cell activation. To integrate the data, we used Forecyt Software's Profile Map data tool in the Panorama feature

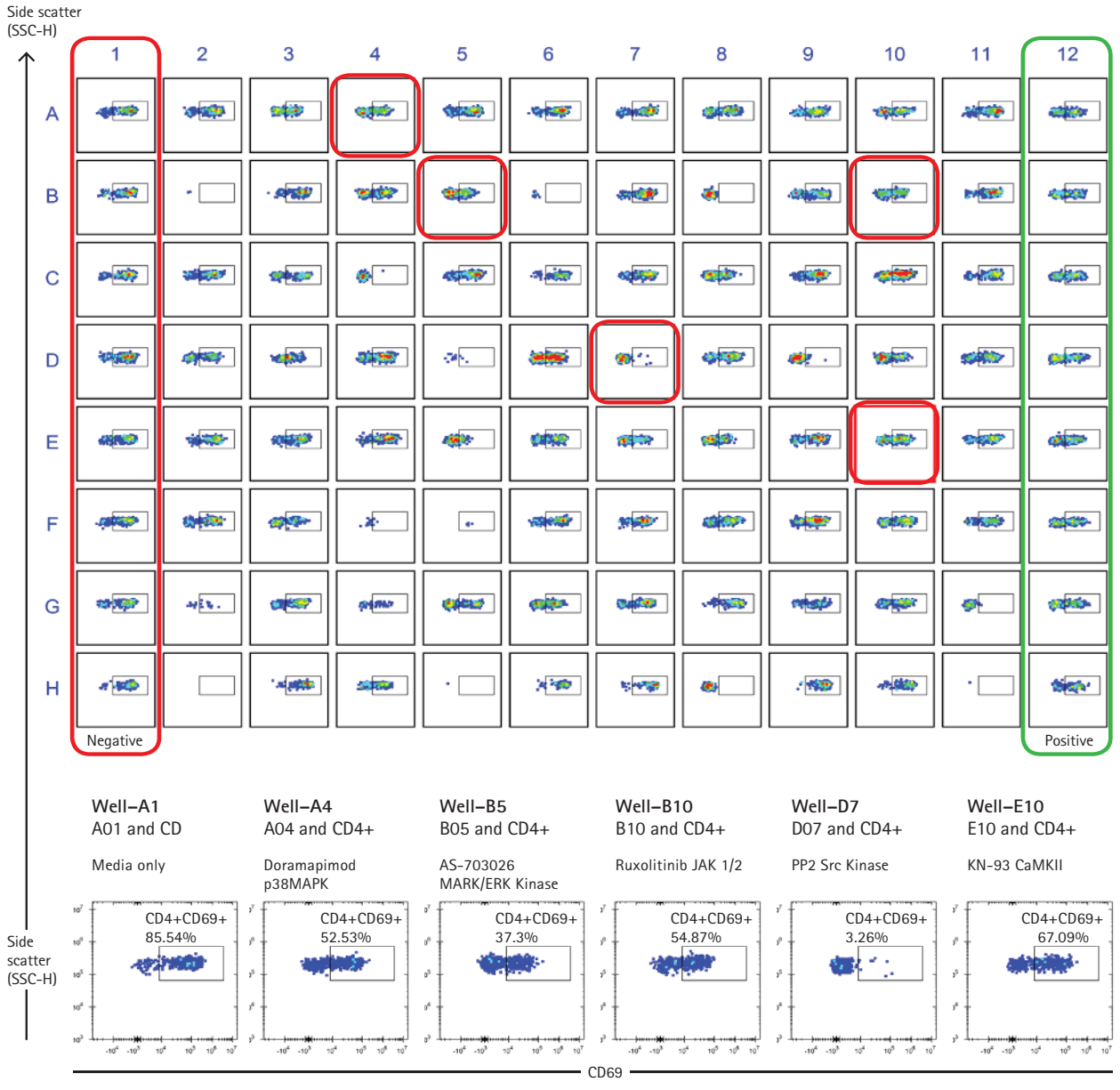

FIG. 5. Compounds that inhibit CD69 expression. A plate-level view (from plate 1) of CD69 expression in T-helper cells was generated in Forecyt software. The CD69 expressing cells are found in the rectangular gate. Wells highlighted in red are shown below with the indicated KI and the % of CD69 CD4+ cells found in the inset of each dot blot.

(Figure 6). The left panel shows the 11 parameters from the screening study that were integrated and the user-defined threshold for each of the metrics. Using the Profile Map, we identified 27 different KI that inhibited expression of all T cell activation markers and cytokine secretion (wells highlighted in blue in Figure 6). The overlay line graph in Figure 6 ranks all of the hits and the level of inhibition, providing easy visualization for each metric. For example, treatment with some KI completely inhibits all activation metrics, whereas other compounds have a greater impact on specific phenotypic markers or cytokines.

By changing the threshold of each parameter, Profile Maps can quickly identify KI that have unique MOA. Shifting the threshold of CD69 expression allowed us to identify two hits that did not affect CD69 expression, but inhibited all other T cell activation markers (Figure 7 and data not shown). This is of importance since CD69 is often the only marker used

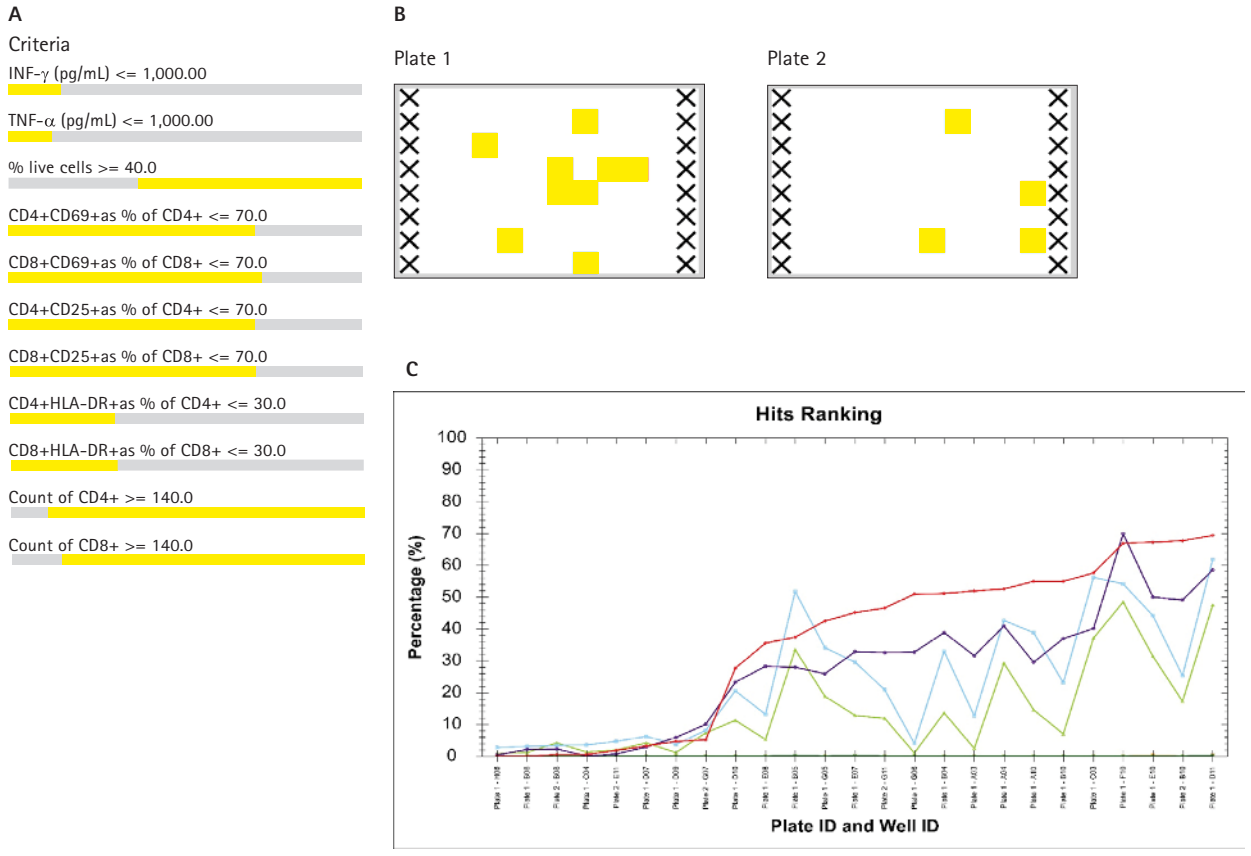

FIG. 6. Profile Maps. To identify hits that inhibited all T cell activation metrics, Profile Maps were generated using the Panorama feature in Forecyt software. The user-defined threshold level of each of the desired metrics is shown in A, while the specific hits from the 2 plates are shaded in blue (B). A line graph ranking the hits based on the % of CD69 CD4+ cells was generated (red line) and line graphs for 5 additional metrics were overlaid for each of the hits. These visualization tools provide easy insight into how the various KI impact different T cell activation metrics.

in many traditional T cell activation panels and these hits would not have been identified. The same strategy was used to identify three KI that did not affect CD25 expression, but inhibited all other metrics and additional compounds that showed differential cytokine secretion (data not shown). Finally, Profile Maps can be used to identify treatments that have similar phenotypes, which is important when trying to compare unknown compounds with drugs that have high safety profiles in the clinic. Using this signature mapping feature in the Profile Map tool, we identified three drugs that showed the same level of inhibition of all metrics as the FDA-approved RA drug Rixinitimab (data not shown). These data illustrate the value of the high-content data generated by Intellicyt's TCA kit and suggest KI can inhibit multiple pathways to inhibit T cell activation.

To confirm the MOA of the KI, and to determine inhibitory concentration curves, a set of compounds were chosen for dose

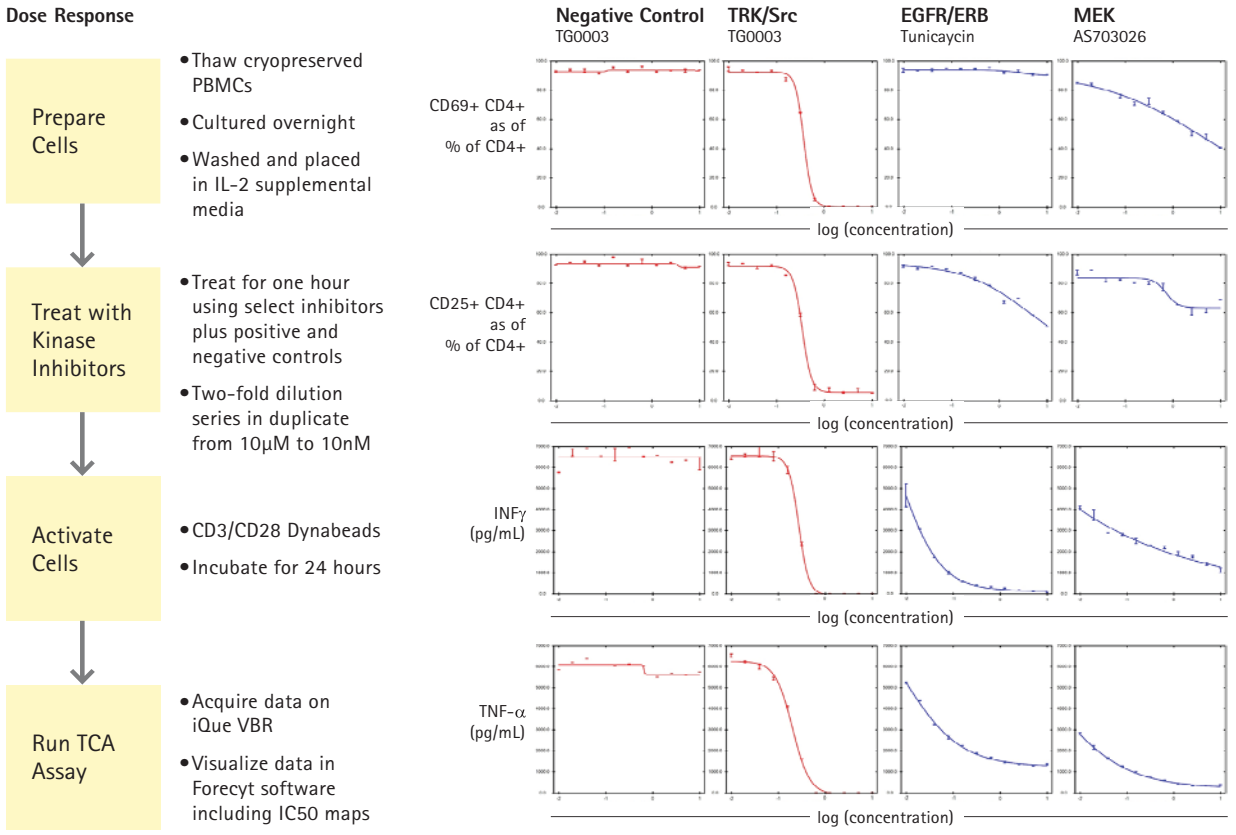

FIG. 7. Dose Response Studies. Select KI were used for dose response studies to confirm MOA and determine IC_{50} concentrations for the various activation and functional markers.

response studies. The protocol for these studies were the same as the initial screen and the concentration ranged from 20 uM to 20nM for all of the compounds (Figure 7). The concentration dependent inhibition of activation and functional markers in the CD4+ population is shown in Figure 7, and all dose response curves and IC_{50} calculations (if required) were generated in Forecyt software. The CHK inhibitor TG003 had no effect on T cell activation. In contrast the receptor tyrosine kinase/src kinase inhibitor PD166326 demonstrated a classic dose response inhibition of all T cell activation markers. The IC_{50} values ranged from 200 – 370 nM for each of the metrics and are shown in the inset of each graph. Tunicamycin, an EGFR/Erb B inhibitor, was a compound identified by the initial screen as a drug that did not affect CD69 expression, but did inhibit other phenotypic and functional markers. This was confirmed in the dose response study where CD69 expression remained

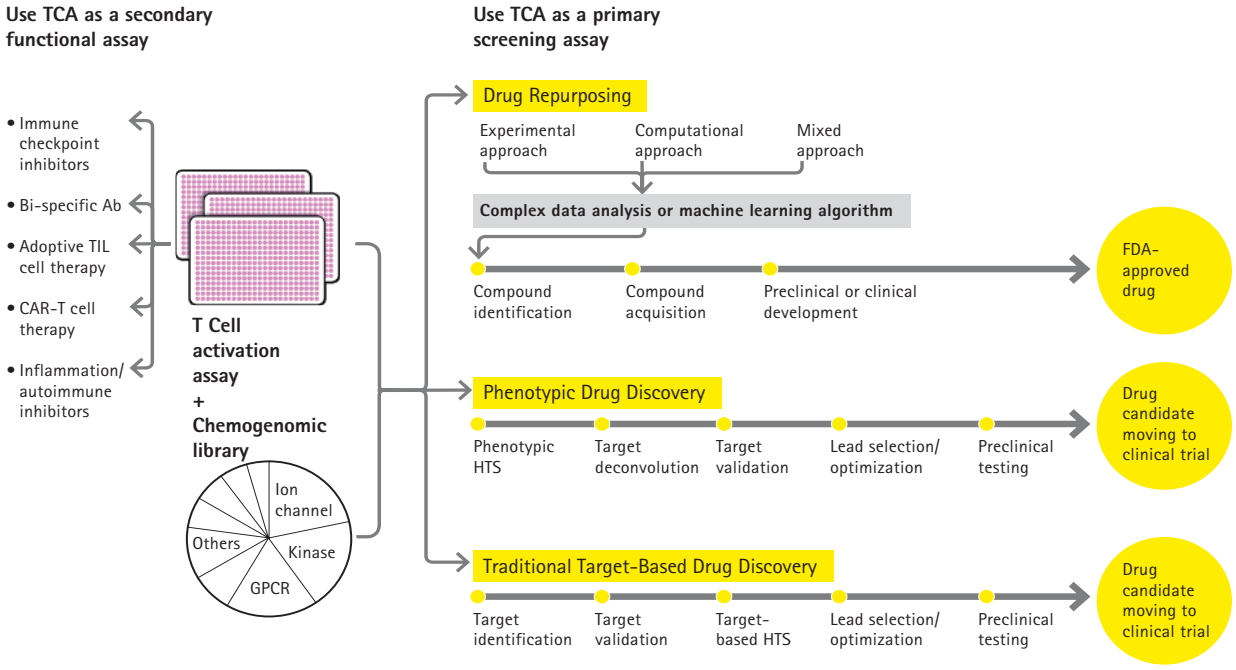

FIG. 8. Position of T cell Activation Cell and Cytokine Profiling Kit in Drug and Biologic Discovery Workflow. The TCA assay can be used as a primary or secondary phenotypic screens in both the biologics and small molecule workflow. Additionally the TCA assay is used for functional studies in the immuno-oncology space and for characterizing T cells during cell manufacturing processes.

unchanged, whereas the percentage of CD25 expressing CD4+ cells were ~50% and little to no INF-g was detected at the high drug concentration. In contrast, the MEK1/2 inhibitor AS703026 showed only a slight decrease in the number of CD25 expressing cells, but a dose response decrease in the other activation metrics. These data show the differences in the MOA of various KI and illustrates the power of Forecyt's visualization and analytic tools to increase biological insight of large data sets.

CONCLUSION

This application notes shows the functionality of the Intellicyt TCA kit for long-term activation assays and in phenotypic drug discovery campaigns. Figure 8 shows the positioning of the TCA kit in the drug discovery workflow. In addition, the TCA kit is applicable to many functional assay workflows including development of checkpoint inhibitors and cell therapies and during cell manufacturing. ■

REFERENCES

1 Navarro MN, & Cantrell DA. **Serine-threonine Kinases in TCR Signaling**, *Nature Immunology* (15) 9 Sept 2014.

2 Gaud G, Lesourne R, and Love PE. **Regulatory Mechanisms in T Cell Receptor Signaling**, *Nature Reviews Immunology* (18) August 2018.

3 Chen EW, Brzostek J, Gascoigne N, and Rybakin V. **Development of a Screening Strategy for New Modulators of T Cell Receptor Signaling and T Cell Activation**, *Scientific Reports* (8) 2018.

4 Reinhold SE, Grimbacher B, and Witte T. **Autoimmunity and Primary Immunodeficiency: Two Sides of the same Coin**, *Nature Reviews Rheumatology* (14) January 2018.

5 Klager S, Heinzlmeir S, Wilheim M et al. **The Target Landscape of Clinical Kinase Drugs**, *Science* (355) December 2017.

6 Ferguson FM & Gray NS. KI: **The Road Ahead**, *Nature Reviews Drug Discovery* (27) 5 May 2018.

7 Moffat J, Vincent F, Lee JA, Eder J and Prunotto M. **Opportunities and challenges in Phenotypic Drug Discovery: An Industry Perspective**, *Nature Reviews Drug Discovery* (16) August 2017.

8 Jones LH & Bunnage ME. **Applications of Chemogenomic Library Screening in Drug Discovery**, *Nature Reviews Drug Discovery* (16) April 2017.

9 Pushpakom, S Iorio F, Eyers PA, et al. **Drug Repurposing: Progress, Challenges and Recommendations**, *Nature Reviews Drug Discovery*, Published Online October 2018.

10 Leitner J, Drobits K, Pickl WF, et al. **The Effects of Cyclolsporine A and Azathioprine on Human T Cells Activated by Different Costimulatory Signals**, *Immunology Letters* (140) 1-2 October 2011.

Antibody Responses to a Quadrivalent Hepatitis C Viral-Like Particle Vaccine Adjuvanted with Toll-Like Receptor 2 Agonists

Dale Christiansen,[1] Linda Earnest-Silveira,[1] Brendon Chua,[1] Irene Boo,[2] Heidi E. Drummer,[1–3] Branka Grubor-Bauk,[4] Eric J. Gowans,[4] David C. Jackson,[1] and Joseph Torresi[1]

1. Department of Microbiology and Immunology, The Peter Doherty Institute for Infection and Immunity, The University of Melbourne, Melbourne, Australia.; 2. Burnet Institute, Melbourne, Australia; 3. Department of Microbiology, Monash University, Clayton, Australia; 4. Department of Surgery, The University of Adelaide and The Basil Hetzel Institute for Translational Health Research, Adelaide, South Australia.

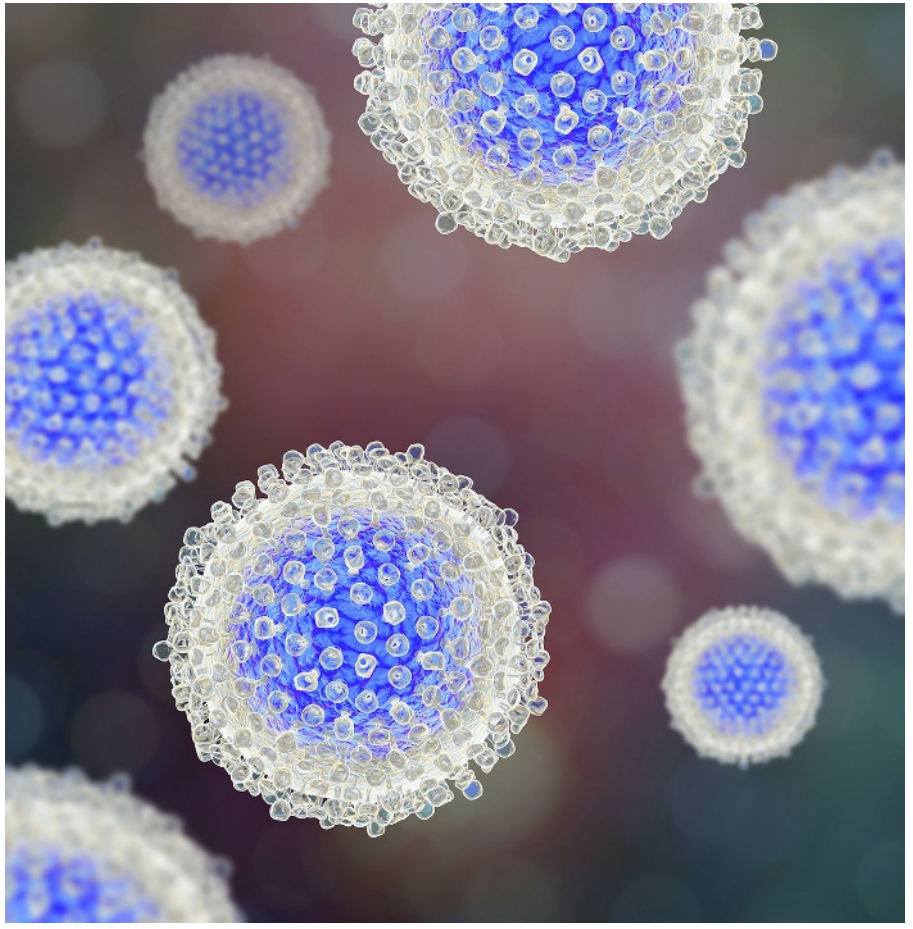

Kateryna Kon / Science Photo Library/Getty Images

ABSTRACT

The development of an effective preventative hepatitis C virus (HCV) vaccine will reside, in part, in its ability to elicit neutralizing antibodies (NAbs). We previously reported a genotype 1a HCV virus like particle (VLP) vaccine that produced HCV specific NAb and T cell responses that were substantially enhanced by Toll-like receptor 2 (TLR2) agonists. We have now produced a quadrivalent genotype 1a/1b/2a/3a HCV VLP vaccine and tested the ability of two TLR2 agonists, R_4Pam_2Cys and E_8Pam_2Cys, to stimulate the production of NAb. We now show that our vaccine with R_4Pam_2Cys or E_8Pam_2Cys produces strong antibody and NAb responses in vaccinated mice after just two

doses. Total antibody titers were higher in mice inoculated with vaccine plus E_8Pam_2Cys compared to HCV VLPs alone. However, the TLR2 agonists did not result in stronger NAb responses compared to vaccine without adjuvant. Such a vaccine could provide a substantial addition to the overall goal to eliminate HCV.

INTRODUCTION

Hepatitis C poses a significant and growing public health problem that will only be partially addressed with the introduction of new antiviral therapies (35). However, reinfection remains a problem in a proportion of individuals who have cleared hepatitis C virus (HCV) (28) and past infection with HCV does not necessarily result in protection against reinfection (1,18,29,34). An effective vaccine would provide a substantial step toward eradicating HCV globally. The efficacy of an HCV vaccine will reside, in part, in its ability to produce broad neutralizing antibodies (NAbs). Cross-NAb responses to epitopes in the viral E2 glycoproteins have been shown to be protective (7,11,31,33), and in humans, the early induction of NAb has been associated with control of viremia, resolution of acute infection (32), and clearance following reinfection (30). In addition, IgG isolated from mice immunized with inactivated cell culture derived HCV has been shown to protect liver chimeric mice against homologous HCV challenge (2).

HCV virus-like particles (VLPs) offer an important approach for the development of a protective vaccine (8,13,24). We have previously reported a human liver cell-derived genotype 1a HCV VLP and characterized the biochemical and biophysical properties and morphology of the VLPs and importantly demonstrated the production of NAb and T cell responses to HCV (8,13). Similarly, a genotype 3a HCV VLP vaccine has also been shown to produce humoral and cellular immune responses (24). To further advance our vaccine approach to cover multiple HCV genotypes we produced a quadrivalent vaccine and established methods for large-scale vaccine production (12). The quadrivalent vaccine includes antigens from four common HCV genotypes: 1a/1b/2a/3a and is expected to produce broader cross-NAb responses and thereby be more effective than a single antigen.

We had previously shown that combining our genotype 1a HCV VLPs with the Toll-like receptor 2 (TLR2) lipopeptide agonists R_4Pam_2Cys or E_8Pam_2Cys as adjuvants resulted in strong antibody responses after just two doses of a monovalent HCV VLP vaccine (8). The TLR2 lipopeptides carry either a net positive (R_4Pam_2Cys) or negative (E_8Pam_2Cys) charge, binding to protein antigens by electrostatic interactions and improving their ability to produce antibody and T cell responses (9). Therefore, we wanted to determine whether the TLR2 agonists also worked well with our quadrivalent vaccine (12).

In this report we show that our quadrivalent vaccine produces strong antibody and NAb responses when combined with novel TLR2 agonists as adjuvants. Our results are encouraging for the development of a protective vaccine for HCV.

MATERIALS AND METHODS

The construction of recombinant adeno-encoding HCV structural protein core E1 and E2 and the large-scale production, purification, concentration, and characterization of our quadrivalent HCV vaccine composed of genotypes; 1a, 1b, 2a, and 3a VLPs have been reported previously (8,12,13).

All animal experiments used 8- to 12-week-old BALB/c mice that were housed in the Doherty Resource Facility under specific pathogen-free conditions. Mice were obtained from the Animal House facility, Department of Microbiology and Immunology, The University of Melbourne. Animal experiments were performed according to local ethics committee approval. Groups of five age- and weight-matched BALB/c mice were immunized subcutaneously on each side of the base of tail with 80 μg (50 μL per dose) of quadrivalent VLP alone, quadrivalent VLP combined with the TLR2 agonists R_4Pam_2Cys or E_8Pam_2Cys (8), or PBS alone (control). The purified HCV VLPs were quantified for total protein (HCV core, E1 and E2) using a Bradford assay (12). Five nanomoles of each TLR2 lipopeptide adjuvant were used per dose of vaccine administered to each mouse. This equated to 9.9 μg for R_4Pam_2Cys and 16.2 μg for E_8Pam_2Cys per dose of vaccine. Two weeks later the mice received a second equivalent dose of quadrivalent vaccine. Animals were sacrificed 1 week after the final immunization, and blood was collected for serum preparation.

Sera were tested by ELISA to determine genotype specific antibody responses. Flat bottom 96-well polyvinyl plates were coated with purified HCV VLPs (20 μg/mL) in carbonate coating buffer (100 mM Na_2CO_3 and $NaHCO_3$, pH 9.6) overnight at 4°C. The plates were then blocked with 100 μL of BSA (10 mg/mL) in PBS and incubated for 2 h at room temperature before washing four times with PBST (PBS containing v/v 0.05% Tween-20; Sigma Aldrich, Milwaukee). Serial dilutions of sera obtained from immunized mice were added to wells and incubated in a humidified atmosphere overnight. After washing, bound antibody was detected using horseradish peroxidase-conjugated rabbit anti-mouse IgG antibodies (Dako, Glostrup, Denmark). Following washing with 3,3′,5,5′-Tetramethylbenzidine (TMB), Liquid Substrate solution (Mabtech) was added to wells for 10–15 min. The reaction was stopped by addition of 50 μL of 0.16 M H_2SO_4. Absorbances were determined on a Labsystems Multiskan Multisoft plate reader at 450 nm. Titers of antibody are expressed as the reciprocal of the highest dilution of serum required to achieve an optical density of 0.2.

Neutralization assays using an HCV infectious cell culture system (HCVcc) using genotype 2a virus have been described previously (6,17). These were performed by mixing HCVcc virus with an equal amount of serially diluted immune serum. Each experiment was performed in triplicate. The virus/serum mixture was incubated for 1 h at 37°C before addition to Huh7.5 cells seeded 24 h earlier at 30,000 cells/well in 48-well plates for 4 h. Cells were washed at least four times and replenished with fresh DMF10NEAA and incubated for a further 48–72 h. Luciferase activity was measured in clarified lysates using Renilla luciferase substrate (Promega) and a FLUOstar OPTIMA microplate reader fitted with luminescence optics (BMG Life Technologies, Germany). The data shown are the mean from at least two independent experiments. Mab24 was used as a positive control for inhibition of HCVcc entry. This monoclonal antibody is a murine NAb that recognizes a linear epitope in the modified recombinant $E2_{661}$ protein that lacks the HVR1, HVR2, and igVR regions (3).

Statistical analysis was performed using the PRISM 5.0 software (GraphPad). In all cases the mean ± standard deviation of the mean (SD) is shown unless otherwise stated. *p* values for statistical analysis were calculated using a one-way analysis of variance. Differences were considered statistically significant when *p* values were less than 0.05 ($p < 0.05$) with a 95% confidence level.

RESULTS AND DISCUSSION

Mice in all vaccination groups developed genotype specific antibody responses (Fig. 1A: a–d). Mice inoculated with quadrivalent VLPs in E_8Pam_2Cys gave the highest genotype specific antibody titers. These were not significantly different than the titers observed with VLPs in R_4Pam_2Cys but were significantly higher than VLP alone (Table 1). The antibody response to the vaccine without adjuvant was still strong and comparable to vaccine supplemented with R_4Pam_2Cys. The strongest responses were detected against HCV genotypes 1a and 1b VLPs, while responses to genotype 2a and 3a VLPs were generally slightly lower across all groups. The geometric mean titer for anti-HCV VLP antibody was highest in mice receiving the quadrivalent HCV VLPs in E_8Pam_2Cys compared to HCV VLPs in R_4Pam_2Cys and HCV VLPs in PBS. These findings were consistent with our previous report showing strong immunogenicity of a monovalent genotype 1a vaccine combined with these TLR2 agonists (8).

We then determined NAb responses to the vaccine using cell culture derived genotype 2a HCV as described in Ref. (37). We compared NAb responses in mice inoculated with quadrivalent vaccine combined with the TLR2 agonists R_4Pam_2Cys or E_8Pam_2Cys. Immune sera were tested at increasing dilutions (Fig. 1B). Sera (diluted 1:30) from mice inoculated with quadrivalent VLPs in R_4Pam_2Cys inhibited HCVcc entry by

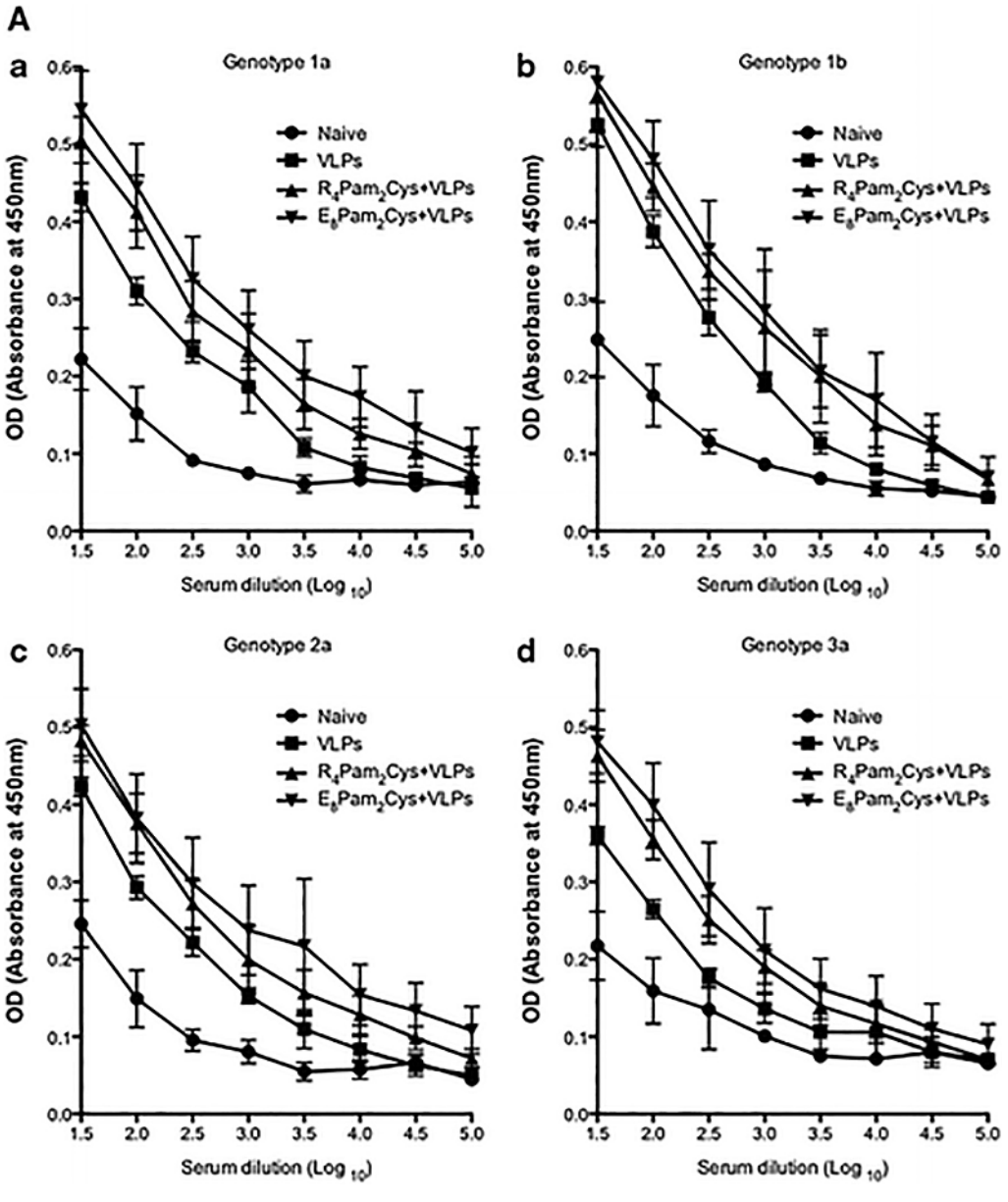

FIG. 1. **(A)** Genotype-specific antibody responses elicited by immunization with quadrivalent vaccines. BALB/c mice (n = 5/group) were immunized subcutaneously at the base of the tail with PBS alone (control) or 80 μg of quadrivalent VLP at a ratio of 1:1:1:1 or quadrivalent VLP combined with 5 nmol of R_4Pam_2Cys or E_8Pam_2Cys in a final volume of 50 μL/dose. Two weeks later the mice received a second equivalent dose of quadrivalent vaccine. Genotype specific antibody in sera prepared from blood taken on day 21 was determined by ELISA using genotype 1a (**a**), 1b (**b**), 2a (**c**), or 3a (**d**) HCV VLPs as coating antigens. In all panels, individual animals are presented for each group, with the mean±standard deviation of the mean (SD) value being represented.
(B) Neutralizing antibody responses to quadrivalent VLP combined with R4Pam2Cys or E8Pam2Cys. Neutralization assays were performed by mixing genotype 2a HCVcc virus with an equal amount of serially diluted immune serum from mice inoculated with quadrivalent VLP alone or combined with R_4Pam_2Cys or E_8Pam_2Cys. The virus/serum mixture was incubated for 1 h at 37°C before addition to Huh7.5 for 4 h. The cells were washed, replenished with fresh DMF10NEAA, and incubated for a further 4–72 h before measuring luciferase activity in clarified lysates using Renilla luciferase substrate (Promega) and a FLUOstar OPTIMA microplate reader. Neutralization was expressed as the percentage inhibition of HCVcc entry into Huh7 cells compared to negative control serum. Mab24 was used as the positive control for inhibition of HCVcc entry. Individual animals are presented for each group, with the mean value being represented by the horizontal

FIG. 1. (cont.)

bar. Results shown are for serum dilutions of 1:30 and 1:150. Each experiment was performed in triplicate, and the data shown are the mean from at least two independent experiments. HCV, hepatitis C virus; HCVcc, HCV infectious cell culture system; VLP, virus-like particle. BALB/c mice (n = 5/group) were immunized subcutaneously at the base of the tail with PBS alone (control) or 80 μg of quadrivalent VLP at a ratio of 1:1:1:1 or quadrivalent VLP combined with 5 nmol of R_4Pam_2Cys or E_8Pam_2Cys in a final volume of 50 μL/dose. Two weeks later the mice received a second equivalent dose of quadrivalent vaccine. Genotype specific antibody in sera prepared from blood taken on day 21 was determined by ELISA using genotype 1a (A), 1b (B), 2 (C), or 3a (D) HCV VLPs as coating antigens. Values represent the geometric mean antibody titer (log_{10}) and 95% confidence interval (shown in brackets) from 5 individual mice per treatment group using individual HCV genotypes; Gt1a, Gt1b, Gt2a, and Gt3a as coating antigens. In all cases, a significant difference ($p < 0.05$) was observed between treatment groups and naive mice. The geometric mean antibody titers were also significantly higher in mice immunized with VLPs plus E_8Pam_2Cys for all genotypes ($p < 0.05$). HCV, hepatitis C virus; VLP, virus-like particle.

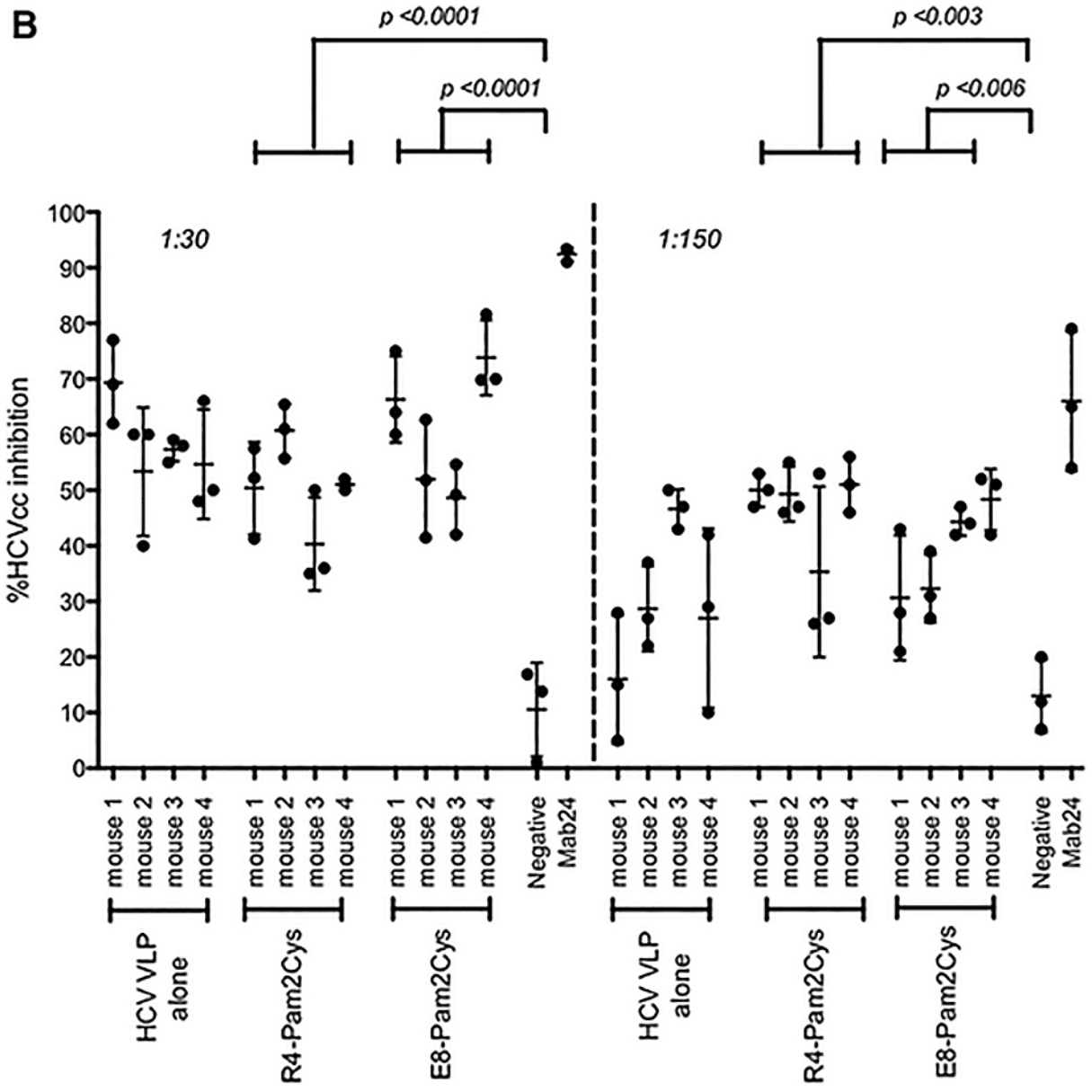

50.6% (±SD 9.3%) compared to 60.2% (±SD 8.4%) with VLPs with E_8Pam_2Cys ($p = 0.02$), 10.6% (±SD 8.4%) ($p < 0.0001$) for negative control sera, and 92.4% (±SD 1.3%) with the monoclonal antibody Mab24 (Fig. 1B). Neutralization of Jc1 HCV was maintained at a serum dilution of 1:150. Sera from mice inoculated with quadrivalent VLPs in R_4Pam_2Cys inhibited HCVcc entry by 46.4% (±SD 9.9%) compared to 38.9% (±SD 9.1%) ($p = 0.04$) with VLPs with E_8Pam_2Cys, 13.0% (±SD 10%) ($p = 0.005$) for negative control sera, and 66.0% (±SD 12.5%) with the monoclonal antibody Mab24 (Fig. 1B). In contrast to the total antibody responses the NAb responses in mice vaccinated with HCV VLPs alone were not significantly lower than in mice vaccinated with adjuvanted HCV VLPs. These findings were consistent with our previous report showing strong immunogenicity of a monovalent genotype 1a vaccine combined with these TLR2 agonists (8).

Table 1. Virus-Like Particle Specific Antibody Titers Elicited by Immunization with Quadrivalent Vaccines

	HCV genotype			
Treatment	***Gt1a***	***Gt1b***	***Gt2a***	***Gt3a***
VLP + E_8Pam_2Cys	3.55 (2.9–4.2)	3.59 (2.3–4.2)	3.43 (2.6–4.2)	3.14 (2.6–3.7)
VLP + R_4Pam_2Cys	3.17 (2.8–3.5)	3.42 (2.9–3.9)	3.05 (2.6–3.4)	2.93 (2.6–3.2)
VLP alone	2.73 (2.5–2.9)	2.90 (2.8–3.0)	2.61 (2.5–3.5)	2.39 (2.3–2.5)
Naive (PBS)	1.63 (1.3–1.9)	1.78 (1.5–2.1)	1.71 (1.5–1.9)	1.62 (1.3–1.9)

BALB/c mice (n = 5/group) were immunized subcutaneously at the base of the tail with PBS alone (control) or 80 μg of quadrivalent VLP at a ratio of 1:1:1:1 or quadrivalent VLP combined with 5 nmol of R_4Pam_2Cys or E_8Pam_2Cys in a final volume of 50 μL/dose. Two weeks later the mice received a second equivalent dose of quadrivalent vaccine. Genotype specific antibody in sera prepared from blood taken on day 21 was determined by ELISA using genotype 1a (A), 1b (B), 2 (C), or 3a (D) HCV VLPs as coating antigens. Values represent the geometric mean antibody titer (log_{10}) and 95% confidence interval (shown in brackets) from 5 individual mice per treatment group using individual HCV genotypes; Gt1a, Gt1b, Gt2a, and Gt3a as coating antigens. In all cases, a significant difference ($p < 0.05$) was observed between treatment groups and naive mice. The geometric mean antibody titers were also significantly higher in mice immunized with VLPs plus E_8Pam_2Cys for all genotypes ($p < 0.05$).
HCV, hepatitis C virus; VLP, virus-like particle.

There are estimated to be a large number of individuals who are unaware that they are infected with HCV, leaving a large residual pool of chronically infected individuals who will act as a persistent source for ongoing HCV transmission (35). An effective preventative vaccine could therefore have a significant impact on HCV prevalence. We have shown that our quadrivalent vaccine results in strong antibody and NAb responses when combined with the TLR2 agonists R_4Pam_2Cys or E_8Pam_2Cys. However, the vaccine was found to be strongly immunogenic after just two doses, even in the absence of adjuvant.

Although a vaccine derived from a single genotype can elicit NAb, the

inclusion of antigens of a number of different genotypes could be expected to produce cross-NAb responses and thereby be more effective than a single antigen. NAbs act by recognizing native E1E2 heterodimers (16), and so an effective preventative vaccine should express native E1E2 structures. The significance of these regions on the viral envelope is further highlighted by the ability of passive immunization with polyclonal and monoclonal antibodies directed to these regions to protect human liver chimeric uPA/SCID mice against challenge with human serum derived HCV (27). In addition, immunization of macaques with a soluble cE2 subunit vaccine has also been shown to induce the production of broad cross NAb (25). These findings are highly significant for HCV vaccine design because they reinforce the need to present both E1 and E2 proteins in the correct structural organization as they would be on virions or HCV VLPs.

The E2 protein contains the major conformational neutralizing antigenic regions (antigenic domains A–E or the AR3 and AR4 regions) organized into distinct clusters of overlapping epitopes (16,20,21). Crystallographic structural analyses of the E2 core domain in complex with key NAbs have helped to define both a neutralizing and a non-neutralizing face to the E2 core antigenic surface (22,23). It has also been possible to map the binding of human monoclonal antibodies (HuMAbs) to these critical regions of E2 with the most potent antibodies binding to domains B and D of the protein (14). These studies reinforce the complex nature of how neutralizing epitopes are presented on the surface of HCV and suggest that these important antigenic regions need to be closely reproduced in a vaccine. A VLP based vaccine should be able to deliver these complex epitopes in the correct conformation.

Peptide epitope antigens can be made more immunogenic when covalently attached to Pam_2Cys to target their delivery through TLR2 to dendritic cells (19). This results in the induction of robust antibody and cell-mediated immune responses (4,10,19,36). We have previously shown that R_4Pam_2Cys and E_8Pam_2Cys enhance the immunogenicity of genotype 1a HCV VLPs, with the improved overall antibody responses compared to VLPs in alum. This study shows that a similar enhancement in antibody responses can be achieved with a quadrivalent HCV VLP vaccine with the TLR2 agonist E_8Pam_2Cys, although this was not significantly greater than quadrivalent HCV VLP in R_4Pam_2Cys or quadrivalent HCV VLP vaccine alone. Studies of the ability of our quadrivalent HCV VLP vaccine to produce cross-NAb responses are currently ongoing using a large animal model.

HCV VLPs elicit both NAb and cellular immune responses (5,8,13,24). Furthermore, as HCV-specific NAbs recognize tertiary or quaternary structures (16), the repetitive and ordered particulate structure of HCV VLPs make them an attractive

vaccine candidate (5,8,15). HCV VLPs are also able to present conformational epitopes in their native state. The development of cross-NAbs to epitopes on the surface of HCV that develop in the course of natural infection provides further encouragement for the development of a neutralizing HCV vaccine (26). An HCV VLP based vaccine would fulfill the requirement of delivering critical conformational neutralizing epitopes, and our report provides further data for the development of a preventative quadrivalent HCV VLP vaccine. ■

ACKNOWLEDGMENTS

This work was supported by the National Health and Medical Research Council (NHMRC) of Australia, grant numbers 1060436 and 1126379. J.T. is supported by an NHMRC Practitioner Fellowship, number 106043.

This work was also supported by Australia-India Biotechnology Research Fund (BF040005), Department of Innovation and Industry, Australian Commonwealth Government.

We wish to thank Prof. Saumitra Das for having provided the cDNA for the production of the HCV genotype 3a VLP vaccine.

AUTHOR DISCLOSURE STATEMENT

No competing financial interests exist.

REFERENCES

1 Aitken CK, Lewis J, Tracy SL, et al. High incidence of hepatitis C virus reinfection in a cohort of injecting drug users. **Hepatology** 2008;48:1746–1752. Crossref, Medline, Google Scholar

2 Akazawa D, Moriyama M, Yokokawa H, et al. Neutralizing antibodies induced by cell culture-derived hepatitis C virus protect against infection in mice. **Gastroenterology** 2013;145:447–455.e1–e4. Crossref, Medline, Google Scholar

3 Alhammad Y, Gu J, Boo I, et al. Monoclonal antibodies directed toward the hepatitis C virus glycoprotein E2 detect antigenic differences modulated by the N-terminal hypervariable region 1 (HVR1), HVR2, and intergenotypic variable region. **J Virol** 2015;89:12245–12261. Crossref, Medline, Google Scholar

4 Alphs HH, Gambhira R, Karanam B, et al. Protection against heterologous human papillomavirus challenge by a synthetic lipopeptide vaccine containing a broadly cross-neutralizing epitope of L2. **Proc Natl Acad Sci U S A** 2008;105:5850–5855. Crossref, Medline, Google Scholar

5 Beaumont E, Patient R, Hourioux C, et al. Chimeric hepatitis B virus/hepatitis C virus envelope proteins elicit broadly neutralizing antibodies and constitute a potential bivalent prophylactic vaccine. **Hepatology** 2013;57:1303–1313. Crossref, Medline, Google Scholar

6 Boo I, teWierik K, Douam F, et al. Distinct roles in folding, CD81 receptor binding and viral entry for conserved histidine residues of hepatitis C virus glycoprotein E1 and E2. **Biochem J** 2012;443:85–94. Crossref, Medline, Google Scholar

7 Broering TJ, Garrity KA, Boatright NK, et al. Identification and characterization of broadly neutralizing human monoclonal antibodies directed against the E2 envelope glycoprotein of hepatitis C virus. **J Virol** 2009;83:12473–12482. Crossref, Medline, Google Scholar

8 Chua BY, Johnson D, Tan A, et al. Hepatitis C VLPs delivered to dendritic cells by a TLR2 targeting lipopeptide results in enhanced antibody and cell-mediated responses. **PLoS One** 2012;7:e47492. Crossref, Medline, Google Scholar

9 Chua BY, Pejoski D, Turner SJ, et al. Soluble proteins induce strong CD8+ T cell and antibody responses through electrostatic association with simple cationic or anionic lipopeptides that target TLR2. **J Immunol** 2011;187:1692–1701. Crossref, Medline, Google Scholar

10 Deliyannis G, Kedzierska K, Lau YF, et al. Intranasal lipopeptide primes lung-resident memory CD8+ T cells for long-term pulmonary protection against influenza. **Eur J Immunol** 2006;36:770–778. Crossref, Medline, Google Scholar

11 Dowd KA, Netski DM, Wang XH, et al. Selection pressure from neutralizing antibodies drives sequence evolution during acute infection with hepatitis C virus. **Gastroenterology** 2009;136:2377–2386. Crossref, Medline, Google Scholar

12 Earnest-Silveira L, Christiansen D, Herrmann S, et al. Large scale production of a mammalian cell derived quadrivalent hepatitis C virus like particle vaccine. **J Virol Methods** 2016;236:87–92. Crossref, Medline, Google Scholar

13 Earnest-Silveira L, Chua B, Chin R, et al. Characterization of a hepatitis C virus-like particle vaccine produced in a human hepatocyte-derived cell line. **J Gen Virol** 2016;97:1865–1876. Crossref, Medline, Google Scholar

14 Fauvelle C, Colpitts CC, Keck ZY, et al. Hepatitis C virus vaccine candidates inducing protective neutralizing antibodies. **Expert Rev Vaccines** 2016;15:1535–1544. Crossref, Medline, Google Scholar

15 Garrone P, Fluckiger AC, Mangeot PE, et al. A prime-boost strategy using virus-like particles pseudotyped for HCV proteins triggers broadly neutralizing antibodies in macaques. **Sci Transl Med** 2011;3:94ra71. Crossref, Medline, Google Scholar

16 Giang E, Dorner M, Prentoe JC, et al. Human broadly neutralizing antibodies to the envelope glycoprotein complex of hepatitis C virus. **Proc Natl Acad Sci U S A** 2012;109:6205–6210. Crossref, Medline, Google Scholar

17 Gottwein JM, Jensen TB, Mathiesen CK, et al. Development and application of hepatitis C reporter viruses with genotype 1 to 7 core-nonstructural protein 2 (NS2) expressing fluorescent proteins or luciferase in modified JFH1 NS5A. **J Virol** 2011;85:8913–8928. Crossref, Medline, Google Scholar

18 Grebely J, Prins M, Hellard M, et al. Hepatitis C virus clearance, reinfection, and persistence, with insights from studies of injecting drug users: towards a vaccine. **Lancet Infect Dis** 2012;12:408–414. Crossref, Medline, Google Scholar

19 Jackson DC, Lau YF, Le T, et al. A totally synthetic vaccine of generic structure that targets Toll-like receptor 2 on dendritic cells and promotes antibody or cytotoxic T cell responses. **Proc Natl Acad Sci U S A** 2004;101:15440–15445. Crossref, Medline, Google Scholar

20 Keck Z, Op De Beeck A, Hadlock KG, et al. Hepatitis C virus E2 has three immunogenic domains containing conformational epitopes with distinct propertires and biological functions. **J Virol** 2004;78:9224–9232. Crossref, Medline, Google Scholar

21 Keck ZY, Li TK, Xia J, et al. Definition of a conserved immunodominant domain on hepatitis C virus E2 glycoprotein by neutralizing human monoclonal antibodies. **J Virol** 2008;82:6061–6066. Crossref, Medline, Google Scholar

22 Khan AG, Whidby J, Miller MT, et al. Structure of the core ectodomain of the hepatitis C virus envelope glycoprotein 2. **Nature** 2014;509:381–384. Crossref, Medline, Google Scholar

23 Kong L, Giang E, Nieusma T, et al. Hepatitis C virus E2 envelope glycoprotein core structure. **Science** 2013;342:1090–1094. Crossref, Medline, Google Scholar

24 Kumar A, Das S, Mullick R, et al. Immune responses against hepatitis C virus genotype 3a virus-like particles in mice: a novel VLP prime-adenovirus boost strategy. **Vaccine** 2016;34:1115–1125. Crossref, Medline, Google Scholar

25 Li D, Wang X, von Schaewen M, et al. Immunization with a subunit hepatitis C virus vaccine elicits pan-genotypic neutralizing antibodies and intra-hepatic T-cell responses in non-human primates. **J Infect Dis** 2017;215:1824–1831. Crossref, Medline, Google Scholar

26 Mancini N, Diotti RA, Perotti M, et al. Hepatitis C virus (HCV) infection may elicit neutralizing antibodies targeting epitopes conserved in all viral genotypes. **PLoS One** 2009;4:e8254. Crossref, Medline, Google Scholar

27 Meuleman P, Bukh J, Verhoye L, et al. In vivo evaluation of the cross-genotype neutralizing activity of polyclonal antibodies against hepatitis C virus. **Hepatology** 2011;53:755–762. Crossref, Medline, Google Scholar

28 Midgard H, Bjoro B, Maeland A, et al. Hepatitis C reinfection after sustained virological response. **J Hepatol** 2016;64:1020–1026. Crossref, Medline, Google Scholar

29 Osburn WO, Fisher BE, Dowd KA, et al. Spontaneous control of primary hepatitis C virus infection and immunity against persistent reinfection. **Gastroenterology** 2010;138:315–324. Crossref, Medline, Google Scholar

30 Osburn WO, Snider AE, Wells BL, et al. Clearance of hepatitis C infection is associated with the early appearance of broad neutralizing antibody responses. **Hepatology** 2014;59:2140–2151. Crossref, Medline, Google Scholar

31 Owsianka AM, Tarr AW, Keck ZY, et al. Broadly neutralizing human monoclonal antibodies to the hepatitis C virus E2 glycoprotein. **J Gen Virol** 2008;89:653–659. Crossref, Medline, Google Scholar

32 Pestka JM, Zeisel MB, Blaser E, et al. Rapid induction of virus-neutralizing antibodies and viral clearance in a single-source outbreak of hepatitis C. **Proc Natl Acad Sci U S A** 2007;104:6025–6030. Crossref, Medline, Google Scholar

33 Raghuraman S, Park H, Osburn WO, et al. Spontaneous clearance of chronic hepatitis C virus infection is associated with appearance of neutralizing antibodies and reversal of T-cell exhaustion. **J Infect Diseases** 2012;205:763–771. Crossref, Medline, Google Scholar

34 Sacks-Davis R, Aitken CK, Higgs P, et al. High rates of hepatitis C virus reinfection and spontaneous clearance of reinfection in people who inject drugs: a prospective cohort study. **PLoS One** 2013;8:e80216. Crossref, Medline, Google Scholar

35 Sievert W, Razavi H, Estes C, et al. Enhanced antiviral treatment efficacy and uptake in preventing the rising burden of hepatitis C-related liver disease and costs in Australia. **J Gastroenterol Hepatol** 2014;29 Suppl 1:1–9. Crossref, Medline, Google Scholar

36 Torresi J, Stock OM, Fischer AE, et al. A self-adjuvanting multiepitope immunogen that induces a broadly cross-reactive antibody to hepatitis C virus. **Hepatology** 2007;45:911–920. Crossref, Medline, Google Scholar

37 Vietheer PT, Boo I, Gu J, et al. The core domain of hepatitis C virus glycoprotein E2 generates potent cross-neutralizing antibodies in guinea pigs. **Hepatology** 2017;65:1117–1131. Crossref, Medline, Google Scholar

SARTORIUS

Simplifying Progress

Accelerate Vaccine Research with Smarter Cell Analysis

Providing you more insights - faster

For tracking complex host-pathogen biological processes, you need cell analysis solutions to generate deeper, more relevant data on phenotype, activation, and function. Sartorius' groundbreaking solutions provide insights at unprecedented speed, depth, and scale with comprehensive analysis and visualization capabilities to get you to actionable results, faster.

Learn more about our solutions at **www.sartorius.com/vaccine-discovery**